To the Graduate Council:

I am submitting herewith a thesis written by Liangcheng Yang entitled “Effect of Ambient Temperature and Humidity on Aging of Nanocarbons.” I have examined the final electronic copy of this thesis for form and content and recommend that it be accepted in partial fulfillment of the requirements for the degree of Master of Science, with a major in Environmental Engineering.

Sandeep Agnihotri, Major Professor

We have read this thesis
and recommend its acceptance:

Terry L. Miller

Qiang He

Accepted for the Council:

Carolyn R. Hodges, Vice Provost and
Dean of the Graduate School

(Original signatures are on file with official student records.)

Effect of Ambient Temperature and Humidity on Aging of Nanocarbons

A Thesis Presented for
the Master of Science
Degree
The University of Tennessee, Knoxville

Liangcheng Yang
August 2009

Copyright © 2009 by Liangcheng Yang
All rights reserved.

Acknowledgement

I would like to express my thanks to Dr. Sandeep Agnihotri who has served as my graduate advisor. His guidance and insights have been extremely valuable to me throughout my research projects. He has always been patient and willing to donate his time to help me when I struggled with a problem. I would also like to thank him for financial support in the two years. My appreciation is also extended to the members of my committee, Dr. Terry L. Miller and Dr. Qiang He for their guidance and suggestions for my thesis.

I also would like to acknowledge all members of the Dr. Agnihotri's group during my stay at UT. It was a pleasure working and interacting with everyone because I developed both professionally and personally. I would like to acknowledge Mr. Pyoungchung Kim for all the guidance and help for instrument operation and research discussion. I would like to thanks to Mrs. Yijing zheng for picking me up from airport, helping me get familiar with life in the new area and teaching me using software.

Special thanks go to Dr. Harry M. Meyer for help me analyzing samples and also go to Dr. Ewa for answering my questions about instrument operation.

Finally, I am also eternally grateful to my parents for instilling in me great values and a positive outlook on life. I love you all the time.

Abstract

We researched effect of ambient temperature and humidity on aging of nanocarbons, including carbon nanotubes and fullerenes. We studied physicochemical properties of these nanocarbons stored in ambient conditions (20°C, 35-55%RH) for 24 months, in 90% relative humidity (RH) environment for 8 months and in 37°C environment for 13 months. We measured surface area and pore volume of samples by using N_2 adsorption (77K) technique and characterized surface chemistry by using X-Ray photospectroscopy and FT-IR spectroscopy. We also analyzed structural defects with Raman spectroscopy. All tests were conducted periodically.

In ambient condition, we found that nanocarbons exhibited a trend of decreasing surface area and pore volume up to 7 to 15 months but then stabilized. We also observed a trend of decreasing surface oxygen from the beginning with much lower % oxygen observed after 12 to 15 months of aging. There was also evidence that structural-defect concentration was lowered. We conclude that nanocarbons are metastable materials, and that their aging in ambient conditions has an unexpected effect whereby oxygen leaves their surface, the structure repairs itself and they become more thermodynamically stable.

Aged nanocarbons (16 months in ambient conditions) were moved to 90% RH environment and 37°C environment. We observed that in 90% RH condition, chemisorption of oxygen and/or water to nanocarbons was enhanced and % oxygen was increased; surface area, pore volume and structural defects were reduced with a trend of

approaching to equilibrium. We conclude that humidity could promote chemisorption of oxygen/water in the air to nanocarbons. We found that in 37°C condition, chemical properties of nanocarbons were only slightly decreased, but their surface area and pore volume were deceased in 1 to 3 months, and then increased in 3 to 13 months. Their physical changes may be related to the temperature dependent thermal expansion which softened intertubular interaction and enlarged spaces between tubes.

This study demonstrated that ambient temperature and humidity play important roles in aging of nanocarbons and also showed that nanocarbons possess differences from bulk carbons in aging. This study could benefit potential applications of nanocarbons and improve understanding long-term environmental impacts of nanocarbons.

TABLE OF CONTENTS

Chapter 1: Introduction 1

1.1 Carbon Nanotubes and Fullerenes C60 1

1.2 Applications of Carbon Nanotubes in Environmental Fields 5

1.3 Environmental Impacts and Human Toxicities of Carbon Nanotubes and Fullerenes 8

1.4 Aging Studies of Carbon 9

1.5 Research Objectives 10

Chapter 2: Methodologies 13

2.1 Sample Description 13

2.2 Sample Characterization 14

2.2.1 N_2 adsorption (77K) Technology 14

2.2.2 XPS 17

2.2.3 Raman 22

2.2.4 FT-IR 25

2.3 Aging environment and timing 28

2.3.1 Aging in the ambient condition 28

2.3.2 Aging with 90% RH and ambient temperature 29

2.3.3 Aging in an oven with 37°C 30

Chapter 3: Results and Discussions 31

3.1 Aging in ambient conditions 31

3.1.1 Fluctuations of physical properties 31

3.1.2 Fluctuations of chemical properties 37

3.1.3 Summary 47

3.2 Aging with 90% RH 48

3.3.1 Fluctuations of physical properties 48

3.3.2 Fluctuations of surface chemistry 50

3.3.3 Summary 55
3.2 Aging at 37 ^{o}C 55
3.2.1 Fluctuations of physical properties 57
3.2.2 Fluctuations of surface chemistry 59
3.2.3 Summary 65

Chapter 4: Conclusions 66

APPENDICES 69

LIST OF REFERENCES 73

VITA 80

LIST OF TABLES

Table 2.1 Properties of selected Nanocarbons 14
Table 2.2 Assignments of infrared absorption peaks to functional groups 26
Table 3.1 Results of functional groups obtained from deconvolution 43
Table 3.2 Records of temperature and humidity in aging oven and lab 56

LIST OF FIGURES

Chapter 1

Figure 1.1 *a.* Electron micrograph showing bundles of single-walled carbon nanotubes which are curved and entangled. *b.* Electron micrograph showing individual single-walled nanotubes..... 2

Figure 1.2 Structure of fullerene C60..... 2

Figure 1.3 Bundled single walled carbon nanotubes. Planform (left) and cross section (right) scanned by transmission electron microscopy (TEM)..... 3

Figure 1.4 Defects within carbon nanotubes: Stone Wale defect (left) and vacancies defect (right)..... 4

Figure 1.5 Defects and attached surface functional groups..... 5

Figure 1.6 Two high-density hydrogen coverage on Ti-coated nanotubes: C_8TiH_8 (left) and C_4TiH_8 7

Figure1.7 Different adsorption sites on a homogeneous bundle of partially open-ended SWNTs: (1) internal, (2) interstitial channel, (3) external groove site, and (4) external surface 8

Chapter 2

Figure2.1 Autosorb1 from Quantachrome Corp. in SERF 702 18

Figure 2.2 N_2 adsorption isotherm (left) and multi-BET method (right) 18

Figure 2.3 Schematic of X-ray photoelectron spectroscopy 19

Figure 2.4 X-Ray Photoelectron Spectroscopy (XPS) in ORNL 19

Figure 2.5 Survey scan spectrum (A) and carbon C1s scan spectrum (B) 20

Figure 2.6 Deconvolution of carbon C 1s spectra..... 22

Figure2.7 Energy level diagram showing the states involved in Raman signal. 23

Figure 2.8 Pellet making process. A: Pellet making instrument; B: sample loading; C: loading pressure; and D: 11 mm pellet..... 24

Figure 2.9 Raman spectrum 25

Figure 2.10 FI-IR spectrum of carbon nanotube 27

Figure 2.11 FI-IR and Raman spectroscopy located in SERF 702 27

Figure 2.12 Aging with 90% RH in ambient temperature: Schematic of aging system (up) and experiment setup (down)..... 29
Figure 2.13 Aging of nanocarbons in an oven with 37 ^{o}C temperature. Aging samples inside of the oven (left) and oven temperature (right) 30

Chapter 3

Figure 3.1 CS40 (left) and BU90 (right). A: BET Surface area and B: Total Pore volume (P/P_0=0.90). 33
Figure 3.2 Sample CS70 (left) and CS80 (right). A: Surface area and B: Pore volume.35
Figure 3.3 Sample MWNT (left) and C60 (right). A: Surface area and B: Pore volume. 36
Figure 3.4 Results of X-ray Photoelectron Spectroscopy: (A) survey spectra of CS70 and (B) summary of oxygen contents in nanocarbons. The error bar represents one standard deviation based on 3 replicates..... 38
Figure 3.5 Functional groups from XPS carbon C1s scan. CS70 (A); CS80 (B); CS40 (C). 0-3 (new) samples were just manufactured and purchased in Feb.2009. 42
Figure 3.6 Results of Raman Spectroscopy: (A) spectra of CS80 and (B) measured Id/Ig in SWNTs under aging. The error bar represents one standard deviation based on 8~10 replicates..... 46
Figure 3.7 Aging of nanocarbons with 90% RH for 8 months. A: Surface area; B: pore volume. 49
Figure 3.8 Oxygen content of nanocarbons in aging with 90% RH for 8 months..... 51
Figure 3.9 Deconvolution of CS70 C1s scan in aging with 90% RH for 8 months. 53
Figure 3.10 Deconvolution of CS80 C1s scan in aging with 90% RH for 8 months. 53
Figure 3.11 Surface chemistry of nanocarbons with aging with 90% RH for 8 months. 54
Figure 3.12 Defects of nanocarbons in aging with 90% RH for 8 months..... 55
Figure 3.13 Aging of nanocarbons with 37°C for 13 months. A: Surface area; B: Pore volume. 58
Figure 3.14 Oxygen contents of nanocarbons in aging with 37°C for 8 months. The error bar represents one standard deviation based on 3 replicates..... 60
Figure 3.15 Defects of nanocarbons in aging with 37 ^{o}C for 8 months. The error bar represents one standard deviation based on 8 replicates..... 62

Figure 3.16 Deconvolution of CS80 XPS C1s scan in aging with 37°C for 8-month..... 62
Figure 3.17 Surface chemistry of nanocarbons in aging with 37 ^{o}C for 8 months..... 63
Figure. 3.18 Raman shift at different temperature 64

Nomenclature

CNTs	Carbon nanotubes
SWNT	Single walled carbon nanotube
DMNTs	Double walled carbon nanotubes
MWNTs	Multi walled carbon nanotubes
BET	Brunauer–Emmett–Teller, a method for calculating solid surface area
RH	Relative humidity
PV	Pore volume
MP	Micro pore, in which pore width is smaller than 2 nm
SA	Surface area
TEM	Transmission Electron Microscopy
XPS	X-ray photoelectron spectroscopy
Raman	Raman spectroscopy
FT-IR	Fourier Transform Infrared spectroscopy

CHAPTER 1

INTRODUCTION

1.1 Carbon Nanotubes and Fullerenes C60

Carbon nanotubes (CNTs) are novel materials. It has been known, researched, and used for only less than 20 years since it was observed by Lijima in 1991. The needle-like carbon tubes (latter were named as carbon nanotubes) were grown on a negative end of carbon electrode, and contained 2-50 graphitic sheets when they were firstly discovered [1]. Two years later, in 1993, Iijima and Ichihashi synthesized single-walled carbon nanotubes (SWNTs) **(Fig. 1.1)** [2]. Nowadays, carbon nanotubes could be manufactured mainly by three techniques: arc-discharge, laser-ablation, and catalytic growth. Atomically, carbon nanotubes are basically rolled graphitic sheet(s), and could be one atom layer, two layers or several layers thick which are known as single, double and multi wall carbon nanotubes respectively, or named as SWNTs, DWNTs, and MWNTs for short [3].

Fullerene C60 was first discovered by Kroto et al. in Rice University in 1985. It was found to be a polygon which contained 60 carbon atoms. Its structure is similar with soccer. It has 60 vertices and 32 faces, 12 of which are pentagonal and 20 hexagonal. The diameter of C60 is about 0.7 nm **(Fig 1.2)** [4, 5].

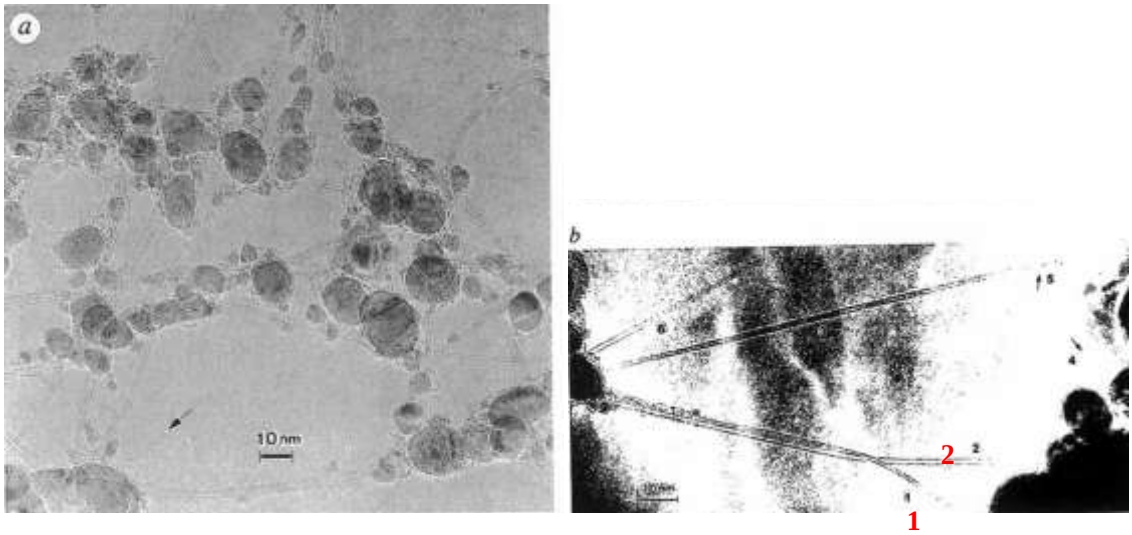

Figure 1.1 *a.* Electron micrograph showing bundles of single-walled carbon nanotubes which are curved and entangled. *b.* Electron micrograph showing individual single-walled nanotubes. The tubule labeled 1 is 0.75 nm in diameter and tubule 2 is 1.37 nm in diameter.

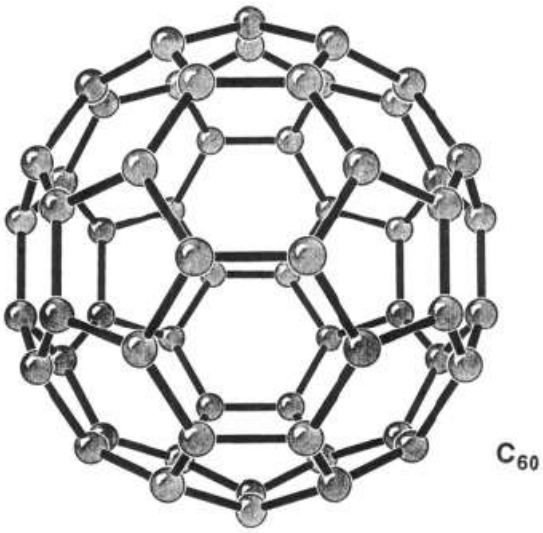

Figure 1.2 Structure of fullerene C60

Carbon nanotubes have unique physical, chemical, mechanical and electronically properties. The nanometric dimension makes them extremely different from bulk materials in physical appearance. Generally, single walled carbon nanotubes (SWNTs) are bundled together **(Fig. 1.3)**, and have a dimension ranging from 0.7 to 1.5 nm in diameter and from 100 nm to 10 µm in length; while multi walled carbon nanotubes (MWNTs) have larger diameter from 5 to 30 nm and varied length from 100 nm to 10 µm [6] depends on manufacturing process and purification methods. The aspect ratio of carbon nanotubes could range from hundreds to millions. With such small dimension, carbon nanotubes have a huge specific surface area and pore volume which could reach as high as 1587 m^2/g and 1.55cm^3/g, respectively [7].

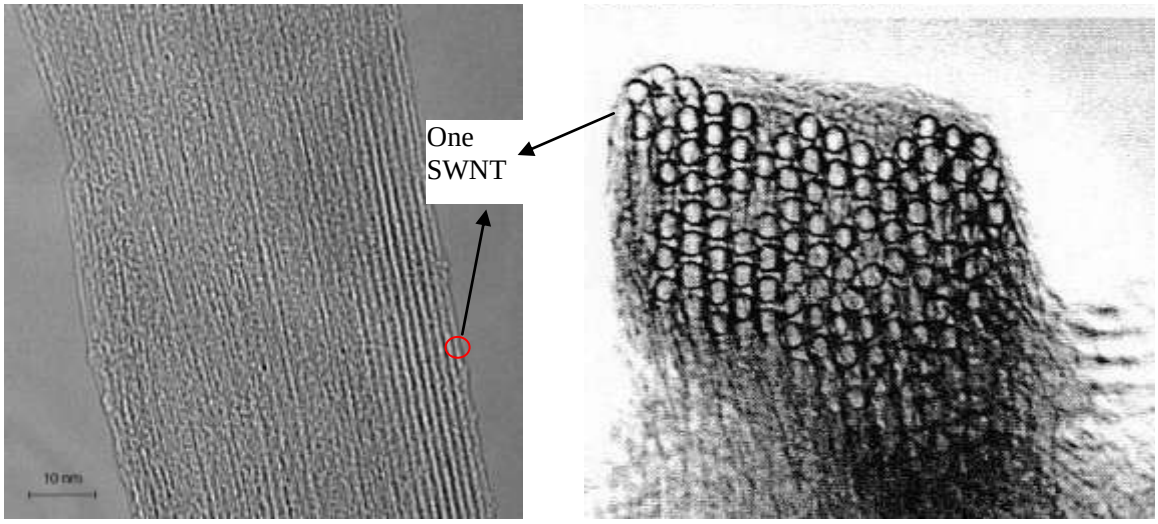

Figure 1.3 Bundled single walled carbon nanotubes. Planform (left) and cross section (right) scanned by transmission electron microscopy (TEM)

Carbon nanotubes could be either metallic or semiconducting depend on its diameter and chirality [8, 9]. In theory, metallic nanotubes can have an electrical current density more than 1,000 times greater than metals such as silver and copper. However, in reality, carbon nanotubes are not perfect hexagon carbon in structure. Defects could occur in the form of atomic vacancies and Stone Wales defects (pentagon and heptagon pair by rearrangement of the bonds) due to the manufacturing and purification process **(Fig. 1.4)** [10]. Defects would weaken the strength of carbon nanotubes and affect their chemical and electrical properties as well. Functional groups like –COOH were found to be more likely attached to these defect sites **(Fig. 1.5)**. The influences of structural defects on properties of carbon nanotubes will be introduced with more detailing description in the following chapters of this thesis.

Carbon nanotubes are also one the strongest and stiffest materials yet discovered on Earth, in terms of tensile strength and elastic modulus respectively [11]. This high strength results from the covalent sp^2 bonds formed between the individual carbon atoms which is even stronger than the sp^3 bonds in diamonds.

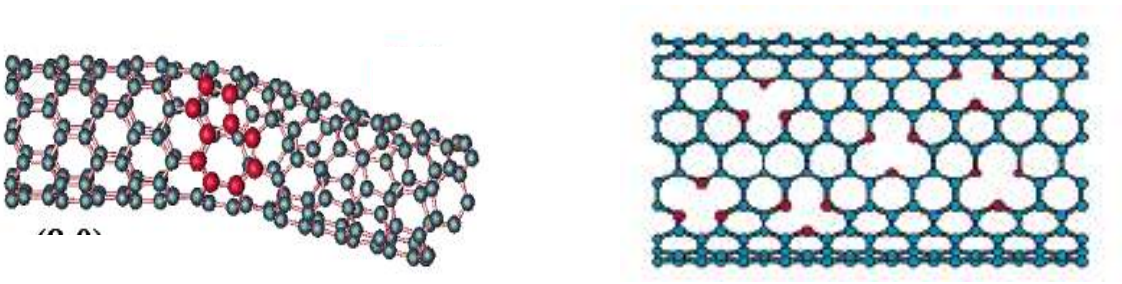

Figure 1.4 Defects within carbon nanotubes: Stone Wale defect (left) and vacancies defect (right).

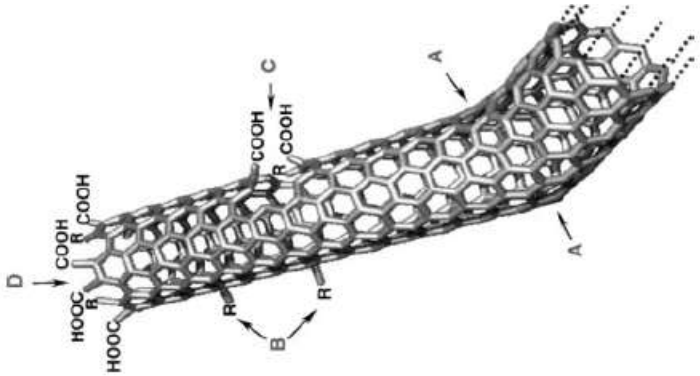

Figure 1.5 Defects and attached surface functional groups

1.2 Applications of Carbon Nanotubes in Environmental Fields

Investigation of properties of carbon nanotubes to develop sensors, store hydrogen and to remove air/water pollutants has attracted much attention from scientists worldwide. Kong at al. found that the electrical resistance of semiconducting SWNT could be dramatically increased or decreased when exposed to gaseous molecules such as NO_2 or NH_3, and nanotubes sensors were demonstrated to have a quick response and much higher sensitivity than existing solid-state sensors at room temperature [12]. Sankaran et al. showed that boron substituted carbon nanotubes could adsorb as much as 2 wt% of hydrogen at 80 bar and 300K [13]; and Yildirim et al. further calculate hydrogen storage of titanium decorated carbon nanotubes and showed that SWNTs can strongly adsorb 5.5wt% hydrogen in the form of C_8TiH_8 and 7.7wt% hydrogen in the form of C_4TiH_8 **(Fig. 1.6)** [14]. Sone and his colleagues observed that carbon nanotubes could be capable of selectively adsorbing aromatic VOCs and the adsorption of the aromatic VOCs can be considered a kind of “soft chemical bonding” interaction [15]. Salipira et al.

worked on pollutants removal from water and they showed that carbon nanotubes can remove organic species such as *p*-nitrophenol by as much as 99% from a 10 mg/L spiked water sample compared to activated carbon and native cyclodextrin polymer that removed only 47% and 58%, respectively [16].

Research into using carbon nanotubes for these applications are primarily motivated by nanotubes having a porous structure which imparts a high adsorption surface area and a large void volume [17]. It has been shown that adsorption capacities of carbon nanotubes can be enhanced either by chemically functionalizing their surface with a host-specific molecular tether capable of binding to a target (in)organic species [18] or by sample heat treatment and annealing which oxidizes the ends of nanotubes and makes their porosity available. Some recent studies have reported that heat treatment at low temperatures (300 ^{o}C to 600 ^{o}C) could increase their adsorption capacity for hydrophobic molecules, including hydrogen, by removing surface functional groups [19] while same at higher temperature (> 1000 ^{o}C) will altering the structure of CNTs, affecting their surface area and porosity [20]. Functionalization of carbon nanotubes by acidification [21] or ozonation techniques [22] is known to increase the concentration of surface oxygen which enhances adsorption of hydrophilic molecules. Previous works have also used theoretical methods to examine chemical adsorption of small gas molecules such as CO, NO, NH_3, N_2, H_2, C_2H_2 and C_2H_4 on Pt coated CNTs, [23] and have compared the migration of hydrogen atoms on Pt surface with that on pristine and defected CNTs [24].

Another important research focused on the adsorption sites of carbon nanotubes.

Agnihotri et al. proposed that purified carbon nanotubes have four sites for adsorption, including internal of the tubes, interstitial sites between tubes, external groove site and external surface of bundles **(Fig. 1.7)** [25]; and other nanometer-thick layered carbon and carbon-coated catalyst particle could also provide adsorption sites [26]. An adsorption modeling approach for heterogeneity of SWNTs was also developed. With this modeling approach, experimental adsorption isotherm could be deconvoluted into several components and qualify adsorption inside the nanotubes, adsorption on the external surface of the bundles, and adsorption on impurities [27].

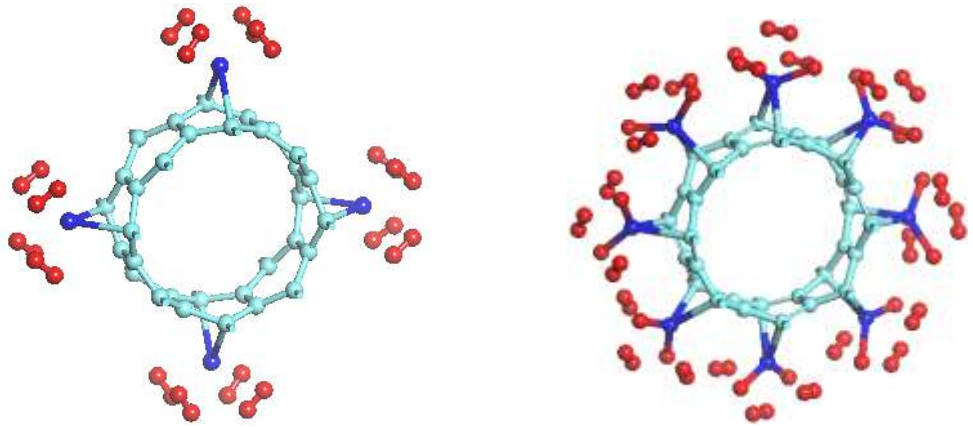

Figure 1.6 Two high-density hydrogen coverage on Ti-coated nanotubes: C_8TiH_8 (left) and C_4TiH_8

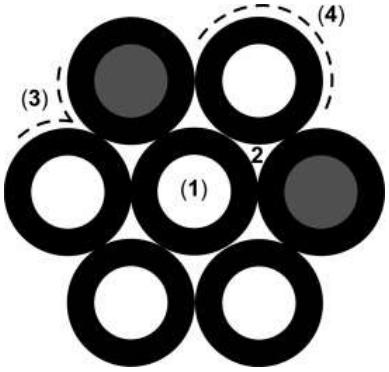

Figure1.7 Different adsorption sites on a homogeneous bundle of partially open-ended SWNTs: (1) internal, (2) interstitial channel, (3) external groove site, and (4) external surface

1.3 Environmental Impacts and Human Toxicities of Carbon Nanotubes and Fullerenes

Carbon nanotubes, both single and multi-walled (SWNTs and MWNTs), and fullerenes are under investigation for their potential impacts on human health or the environment [28]. The nanometric scale enables these materials to penetrate biological tissues [29]. This property allows them to damage human skin [30], respiratory tract [31] and nervous system [32]. The cytotoxicity of nanocarbons is now known to follow the sequence of SWNT > MWNT > C60 [33], and surface area is demonstrated to be the best physicochemical property to predict potential toxicity of nanocarbons [34]. Shvedova et al. found oxidative stress and cellular toxicity when a cell culture of immortalized human epidermal keratinocytes was exposed to SWNTs [35]. Lam et al. studied pulmonary toxicity of SWNTs using mice and observed dose-dependent epithelioid granulomas [36]. Oberdorster demonstrated that these ultra fine particles could also target central nervous system [32]. The chemistry of these materials is equally

critical to evaluating their potential environmental impacts. Sayes et al. showed that functionalization of fullerenes by hydroxyl groups increases water solubility and decreases the potential for induced toxicity [37]. Side-wall functionalization of SWNTs was also found to make them less cytotoxic [38]. Kang et al. also showed that toxicity of MWNTs would change after physicochemical modifications by dry oxidation, acid treatment, functionalization and annealing [39]. Other environmental impacts, including airborne inorganics, climate change and acidification induced by three main SWNTs manufacturing processes were assessed by Meagan's group and besides, they found that that energy consumption was a major concern within life circle impacts of SWNTs [40]. Wiesner et al. stated that long-range atmosphere transport of nanomaterials is possible and their cycling may involve photochemical reactions in the atmosphere [41]. Fates of nanocarbons were also of crucial importance. It was showed that MWNTs could accumulate in liver of mice and retained there for a long time [42]; functionalized SWNTs are of high solubility in aqueous solutions [43]; and MWNTs were relatively stable in aquatic environmental with typical pH and electrolyte conditions [44]. In all, the unique physicochemical properties enable nanocarbons to retain in various environments for a long period of time and would continuously cause serious environment and health problems.

1.4 Aging Studies of Carbon

It has been clearly evidenced that physicochemical properties of nanocarbons (SWNTs, MWNTs and fullerenes) are the main determinants for their potential applications and environmental impacts [34, 39], but, to date, most research focused on

evaluation of the performance of various treatments and applications within a short period of time, little has been known about how nanocarbons would behave in a long term aging process. Several early studies have estimated aging of non-nanometric carbons including activated carbon and carbon sieve. They reported that activated carbon uptake oxygen in both H_2O-free and humid air conditions within 60 days with a little increase observed thereafter [45]; irreversible chemisorption of oxygen happened to carbon molecular sieve membrane when it was aged in air or pure oxygen with a trend of approaching to equilibrium [46]; also, permeance of carbon membrane was noticed to be degraded because of chemisorption of oxygen during aging process [47]; and the simultaneous presence of free oxygen and water vapor, even at room temperature (RT), may react with oxygenated groups of activated carbon in evolving CO_2 and therefore drastically affect the physical and chemical properties of activated carbon [48]. Our previous research on SWNTs demonstrated that physical properties of SWNTs were unstable in ambient conditions even several months after manufacturing [49]; Sayago et al. also observed that the one-year ambient condition aged SWNT based sensor had a higher hydrogen response, and he concluded that SWNTs may experience slow but progressive structural and chemical changes during aging [50]. Therefore, most likely, the physicochemical properties of nanocarbons were not stable and neither were their environmental impacts. Given the widely interests risen from nanocarbons, there is a clear gap between the application of nanocarbons and the aging effect on nanocarbons.

1.5 Research Objectives

In this study, we aged carbon nanotubes and fullerenes in three different conditions

and investigated the effect of ambient temperature and humidity on physicochemical properties of these nanocarbons in aging. Carbon nanotubes and fullerenes were aged for up to 24 months in ambient conditions; carbon nanotubes were aged under 90% relative humidity with ~20°C for 8 months, carbon nanotubes were also aged in a 37°C oven with normal humidity for 8 month. Within this research, we observed how aging environments affect the physicochemical properties of carbon nanotubes and fullerenes. Several fundamental physicochemical properties of nanocarbons including surface area, pore volume, structural defects and surface oxygen were tracked periodically. We found that these properties change as the sample ages, and the aging effects in nanocarbons were quite different from those reported for activated carbons and carbon molecular sieves, which is most likely due to the former being a 1-D material and that latter being bulk materials. This new information about the property of nanocarbons can help resolve some of the conflicting reports about environmental impacts of nanocarbons [51]. As an example, the pulmonary toxicity of SWNTs is a subject of debate. Lam et al. (2004) reported that SWNTs (HiPco sample) induced epithelioid granulomas and prebronchial inflammation in rats and therefore pose significant risks to humans [36]. Warheit et al (2004) conducted a similar study on SWNTs (DuPont sample). They observed granulomas but not prolonged inflammation, and concluded that the toxicological information may be less relevant to humans [52]. Motivated by these two reports Shvedova et al. (2005) from NIOSH conducted an independent study. They concluded that SWNTs (HiPco sample) are toxic and pose a risk of causing lung lesions [53], in general agreement with Lam et al. (2004). These and multiple other studies adhere to the highest standards of experimental protocols but may not be able to reproduce results

from a previous work because a nanocarbon had unknowingly aged while being stored in a normal laboratory environment.

CHAPTER 2

METHODOLOGIES

2.1 Sample Description

In this study, five SWNT samples (CS40, CS70, CS80, BU80, and BU90), one MWNTs sample, and one fullerene (C60) sample were researched **(Table 2.1)**. CS40, CS70, CS80 were purchased from Carbon Solutions Inc. in Sep.2006 (Riverside, CA) and were manufactured by electric arc method. CS40 was as-prepared sample containing high content of metal catalysts; CS70 was manufactured by the same method as CS40 but was purified by air oxidation to remove catalysts and was left with low functionality and low chemical doping; CS80 was also same kind of material as CS40 but was purified with nitric acid and remained with highly functionalized form. It contained 4-6 atomic% carboxylic acids. BU80 and BU90 were chemical vapor deposition (CVD) synthesized samples and were obtained from BuckyUSA Inc. (Houston, TX) in Sep. 2006. BU80 was an as-produced sample while BU90 was a purified sample. Multi-walled carbon nanotubes (CVD method) and fullerenes were purchased from MER Corp. (Tucson, AZ) in Sep. 2006 and were of high purity. Sample details are summarized in following table.

Table 2.1 Properties of Selected Nanocarbons

CNTs		diameter (nm) [a]	length (μm)	aspect ration	purity (wt%) [b]	RM (wt%) [c]
	CS40	1.4	3±2	2143	40-60	30
	CS70	1.4	1.0±0.5	714	70-90	5-10
SWNT	CS80	1.4	1.0±0.5	714	80-90	4
	BU80	0.85, 0.95 1.17,	-	-	80-90	
	BU90	1.32, 1.67	2.5±2	1894,1497	>95	5
Fullerene (C60)		N/A	N/A	N/A	> 99.9	N/A
MWNTs		35±10	30	857	> 90	< 1

[a] determined by Raman scattering. [a,b,c] provided by manufacturer. [c] Residual mass after thermo-gravimetric analysis (TGA) in the air. Major metal catalyst residual in SWNTs are nickel and yttrium, and in MWNTs is Fe.

2.2 Sample Characterization

In this study, several instruments were applied. Standard N_2 adsorption (77K) technology was used for physical properties analysis (located in SERF building 702, UT); X-ray photoelectron spectroscopy (XPS) (one in Material Science department, UT and another one in ORNL), Fourier Transform Infrared (FT-IR) spectroscopy and Raman spectroscopy (located in SERF building 702, UT) were used for chemical properties analysis.

2.2.1 N_2 adsorption (77K) Technology

N_2 adsorption (77K) technology is widely used to analyze physical properties of materials. N_2 is used as a probing molecule to cover the surface of materials to obtain information including surface area, pore volume, pore size distribution, and so on. The adsorption isotherm is obtained when the relative pressure of adsorbate (N_2) is increased generally (10^{-6} to 0.99 in this study), and isotherm then is analyzed using

Brunauer–Emmett–Teller (BET) method. The BET theory sets a theoretical basis for calculating the surface area of the solid. The theory was derived on the assumptions that (1) the Langmuir equation applies to each adsorbed layer (i.e., the surface has uniform and localized sites so that there is no interference in adsorption between neighboring sites); (2) the adsorption and desorption occur only onto and from the exposed layer surfaces; (3) at solid–vapor equilibrium, the rate of adsorption onto the *i*th layer is balanced by the rate of desorption from the (*i* + 1)th layer; and (4) the molar heat of adsorption for the first layer is considered to be higher than for the succeeding layers, the latter assumed to be equal to the heat of liquefaction of the vapor [54]. These considerations lead to an isotherm of the form:

$$\frac{Q}{Q_m} = \frac{C_x}{(1-x)[1+(C-1)x]}$$

where Q is the amount of vapor adsorbed at relative vapor pressure $x = P/P_0$, P the equilibrium pressure of the vapor, P_0 the saturation pressure of the vapor at the system temperature, Q_m the (statistical) monolayer capacity of the adsorbed vapor on the solid, and C is a constant related to the difference between the heat of adsorption in the first layer and the heat of liquefaction of the vapor. This equation may be transformed into

$$\frac{x}{Q(1-x)} = \frac{(C-1)x}{CQ_m} + \frac{1}{CQ_m}$$

A plot of $x/[Q(1 - x)]$ versus x should yield a straight line (usually, at $0.05 < x < 0.30$), with a slope of $(C - 1)/CQ_m$ and an intercept of $1/CQ_m$, from which C and Q_m can be determined. The linear relation of $x/[Q(1 - x)]$ versus x usually does not go beyond $x > 0.30$, much because the multilayer adsorption does not proceed indefinitely as the theory

contends. Once Q_m is determined, and if the molecular area of the vapor is known, the total surface area (S_t) of the adsorbent can then be calculated:

$$S_t = \frac{Q_m N A_{cs}}{M}$$

Where N is Avogadro's number (6.023 X 10^{23} molecules/mol); M is the molecular weight of the adsorbate; and A_{cs} is the cross-sectional area of N_2, which is 16.2 $Å^2$ at 77 K. Therefore, the specific surface area of samples could be obtained by simply calculation:

$$S = S_t / w$$

Here *w* is the weight of sample.

The total pore volume is derived from the amount of vapor adsorbed at a relative pressure close to unity, by assuming that the pores are then filled with liquid adsorbate. If the solid contains no macropores the isotherm will remain nearly horizontal over a range of P/P_0 approaching unity and the pore volume is well defined. However, in the presence of macropores the isotherm rises rapidly near P/P_0 = 1 and in the limit of large macropores may exhibit an essentially vertical rise. The volume of nitrogen adsorbed (V_{ads}) can be converted to the volume of liquid nitrogen (V_{liq}) contained in the pores using following equation:

$$V_{liq} = \frac{P_a V_{ads} V_m}{RT}$$

In which P_a and T are ambient pressure and temperature, respectively, and V_m is the molar volume of the liquid adsorbate (34.7 cm^3/mol for nitrogen) [55].

In this study surface area and pore volume of nanocarbons were analyzed by applying the standard N_2 (77K) adsorption technology by using Autosorb1 brought from Quantachrome Corp.**, (Fig. 2.1)**. A small amount of sample (~30 mg) was loaded into a quartz cell to be outgassed at vacuum condition with temperature of 100-600°C for at least three hours to remove humidity and temporarily adsorbed pollutants. Sample was then cooled down to room temperature before doing nitrogen sorption. Nitrogen (UHP N_2, 99.9995% pure) adsorption was run at 77K and relative pressure of 10E-6 to 0.99 to obtain isotherms. Cross-section and non-ideality parameters of nitrogen were set as 16.2Å^2/molecure and 6.580e-5, respectively. Multi-point BET (Brunauer-Emmett-Teller) method and t-method were applied to calculate total surface area and micro surface area/pore volume, respectively, with relative pressure from 0.05 to 0.30 which was recommended by the instrument provider; relative pressure of 0.90 was selected to calculate total pore volume **(Fig. 2.2)**.

2.2.2 XPS

X-ray photoelectron spectroscopy (XPS) is a surface analytical technique, which is based upon the photoelectric effect [56]. Each atom in the surface has core electron with the characteristic binding energy that is conceptually equal to the ionization energy of that electron. When an X-ray beam directs to the sample surface, the energy of the X-ray photon is adsorbed completely by the core electron of an atom. If the photon energy, $h\nu$,

Figure2.1 Autosorb1 from Quantachrome Corp. in SERF 702

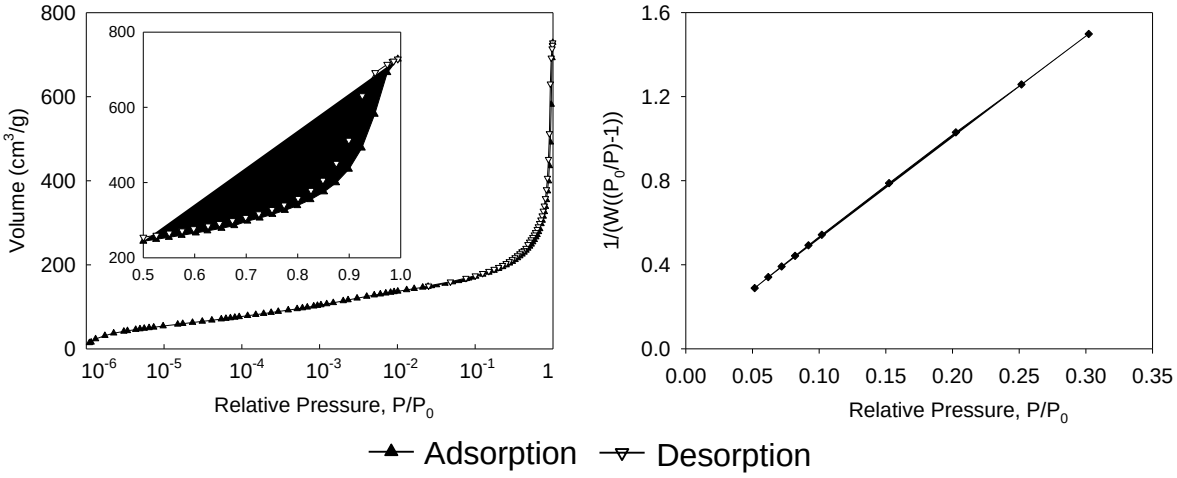

Figure 2.2 N_2 adsorption isotherm (left) and multi-BET method (right)

is large enough, the core electron will then escape from the atom and emit out of the surface. The emitted electron with the kinetic energy of E_k is referred to as the photoelectron. The binding energy of the core electron is give by the Einstein relationship:

$$E_b = hv - E_k$$

Where hv is the X-ray photon energy; E_k is the kinetic energy of photoelectron, which can be measured by the energy analyzer **(Fig. 2.3)**.

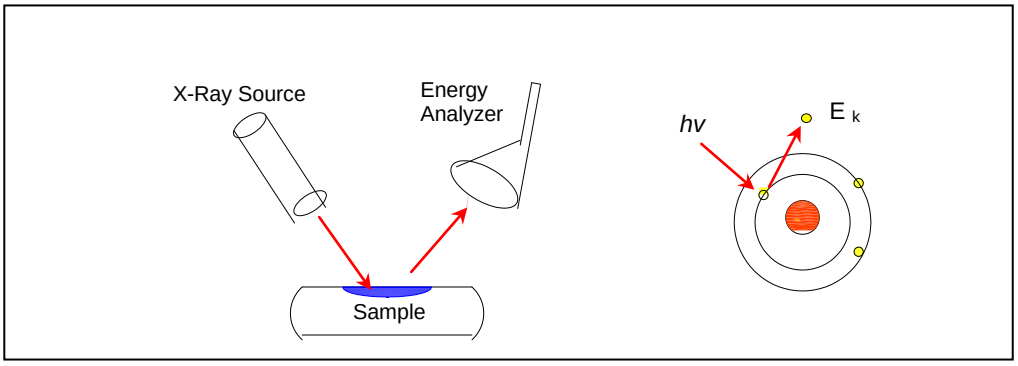

Figure 2.3 Schematic of X-ray photoelectron spectroscopy

Figure 2.4 X-Ray Photoelectron Spectroscopy (XPS) in ORNL

In our study, XPS analysis was conducted in The University of Tennessee, Knoxville (UT) and the Materials Science and Technology Division of Oak Ridge National Laboratory (ORNL) (**Fig. 2.4)**. In ORNL, small sample powders were deposited on a silicon substrate and spectra were collected by using monochromatic Al K-alpha X-ray source, with a power voltage of 12 kV. The X-ray spot size was set as 400 microns and base pressure of the system was maintained at 4E-9 mBarr. Passing energy was controlled at 200 ev for survey scan and 25 ev for narrow region scans (C1s, O1s). In UT, the spectra were collected using the 04-548 Dual Anode (Mg/Al) Kα X-ray source; at an 89.45 eV pass energy for both survey scan and narrow region scans (C1s, O1s) with a power of 300 W, 15 kV. The base pressure of the system was normally maintained below 10-9 Torr. Element contents, including oxygen, carbon and metal catalysts (Cr, Fe, Yi, et al.), could be obtained from survey scan **(Fig. 2.5A)**; the concentrations of oxygen contained functional groups could be extracted out of deconvolution of carbon C 1s scan spectrum **(Fig. 2.5B)**.

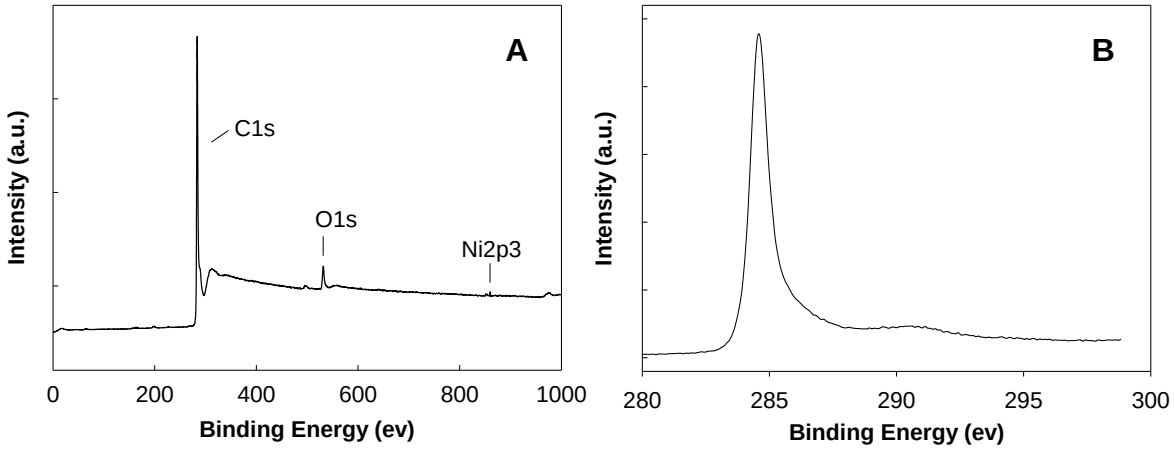

Figure 2.5 Survey scan spectrum (A) and carbon C1s scan spectrum (B)

XPS carbon C1s scan spectrums are deconvoluted into separated peaks by applying well accepted method to get the concentrations of surface functional groups **(Fig. 2.6)** [57-59]. The main peak located at ~284.6 eV, is widely accepted as graphite sp^2 peak; peak at 285.4 ± 0.1 eV is recognized as graphite sp^3 or $sp^{2.x}$. In the right shoulder of main peak with binding energy of 286± 0.1, 287.4± 0.1, 288.9± 0.1 eV and 290.5± 0.1 eV are assigned as -C-O, -C=O, -COOH and π peak respectively. On the left side of main shoulder, a carbon-metal bond is also taken into consideration in our research. Since Ni is the main catalyst used during manufacturing process and remained within these researched samples, therefore, a -C-Ni peak is added, its location is around 283.5 to 283.7 eV. FWHM of -C-O, -C=O, -COOH peaks were controlled at the same value and FWHM of sp^2 and sp^3 peaks were also close to each other, because these function groups and defects sites are supposed to evenly located. However, we find that FWHM of function groups and FWHM of sp^2, sp^3 peaks are not always the same, it may because functional groups attached only on the surface, while XPS is able to penetrate to 5 nm, which makes the difference. This deconvolution method is mainly used for CNTs, and there are few reports that have ever used this deconvolution method to analyze C60 [60]. We think it is also applicable to C60, since C60 is also basically carbon with sp^2 peak, and functional groups could also adhere to its surface. A list of papers about functional group assignments is given in Appendix I.

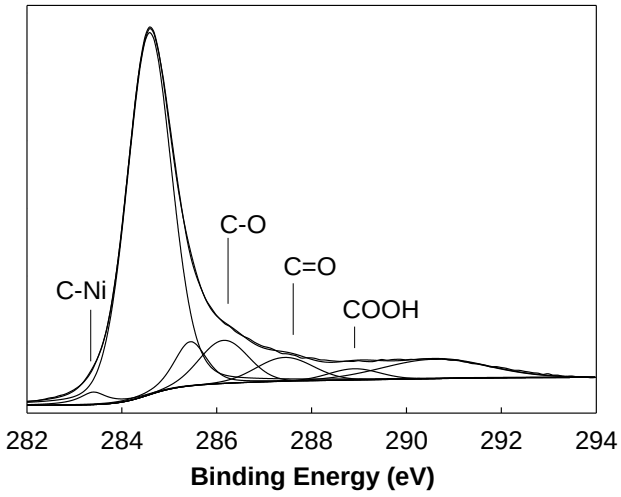

Figure 2.6 Deconvolution of carbon C 1s spectra

2.2.3 Raman

Raman spectroscopy is a nondestructive light scattering technique **(Fig. 2.7)** [61]. It requires the sample to be placed in the path of an excitation beam. It collects the scattered light. It is very powerful tool that is often used to investigate the modifications in the atomic arrangements of carbon nanotubes, especially SWNT. In the using of Raman spectroscopy, the photon excites one of the electrons into a virtual state. When the photon is released the molecule relaxes back into its original vibrational energy state. Raman scattering is only a small fraction of the scattered light, which is about 1 in 1 million photons. Most of the photos scattered as Rayleigh scattering (black line with arrow in Figure). The molecule will typically relax into the first vibrational energy state, and this generates Stoke Raman scattering (green line with arrow in Figure). If the molecule was already in an elevated vibrational energy state, the Raman scattering is then called Anti-Stokes Raman scattering (purple line with arrow in Figure). In the experiment of Raman spectroscopy, the change of the molecular polarizability could be

used to determine the intensity of Raman scattering (Y – axis of spectra), and the Raman shift(X – axis of spectra) is equal to the vibrational level that is involved [62].

In this study, NXR FT-Raman (λ = 976 nm) was applied to analyze surface defects within samples. Samples were grinded with KBr (~0.05 wt%), and then ~100 mg mixed powder was used to make 11mm-diameter transparent pellets with 12000 lbf pressure for 4 minutes **(Fig. 2.8)**. the loading pressure was increased at 6000lbf/min in the beginning two minutes, and was then maintained at 12000 lbf for another two minutes. A sample pellet is shown in following figure. Pellets were tested by Raman with Ge-detector at 0.06W power rating and liquid nitrogen was used to cool down the detector. Pellets were auto-focused and each spot was scanned 32 times. A blank sample (pure KBr) was used to counteract environmental influence.

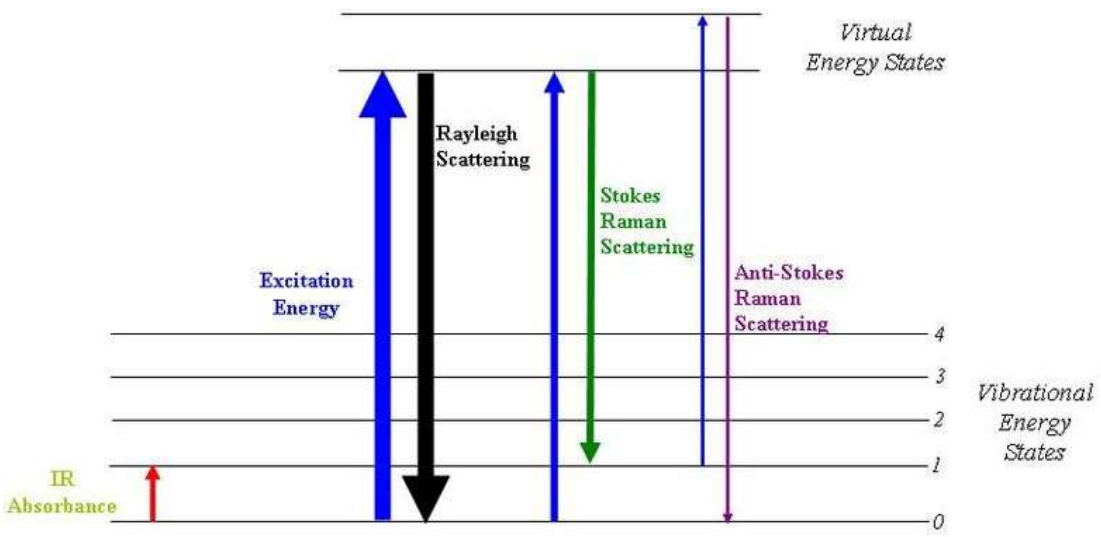

Figure2.7 Energy level diagram showing the states involved in Raman signal.

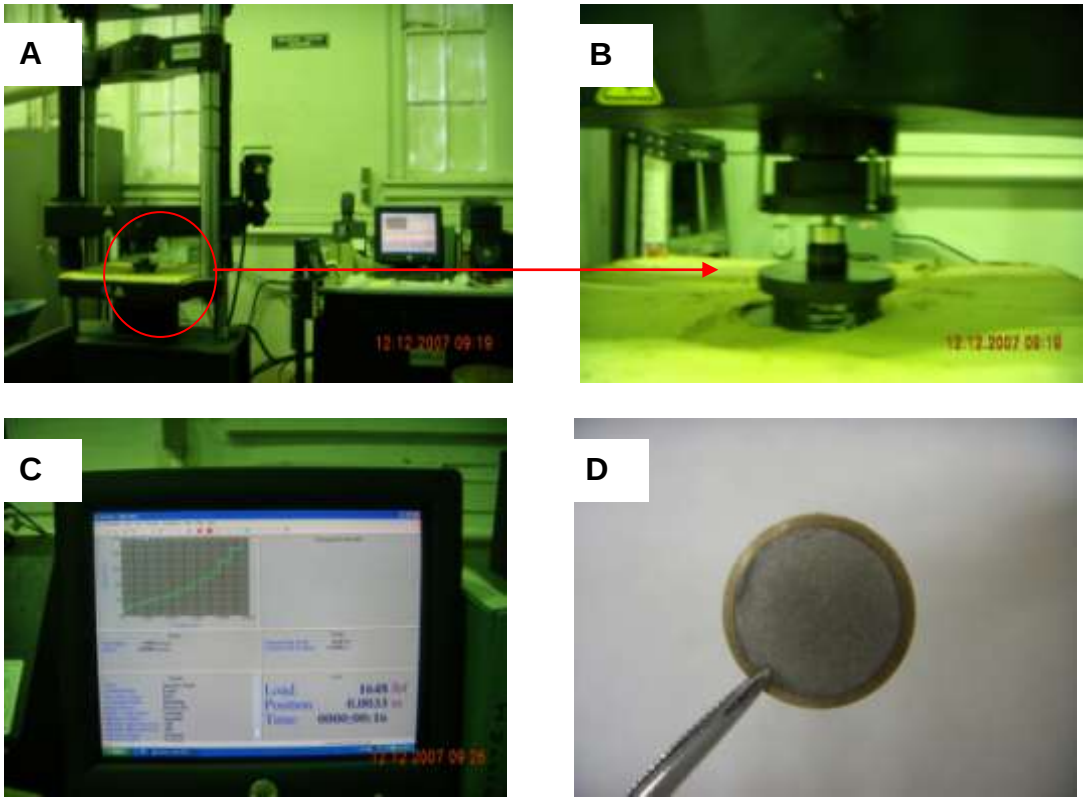

Figure 2.8 Pellet making process. A: Pellet making instrument; B: sample loading; C: loading pressure; and D: 11 mm pellet.

Raman spectrums were widely used to analyze defects in carbon nanotubes. In particular, peak with Raman Shift of ~1320 cm^{-1} is assigned as Disorder (D peak), which is related to structure defects, such as cavity, tips, et al. **(Fig. 1.4)**, carbon atoms in these defective sites could form sp^3 bonds; peak with Raman Shift of ~1600 cm^{-1} is well recognized as Graphite (G peak), carbon atoms in graphite are basically considered as perfect hexagon structure and normally have sp^2 bonds. Therefore, ratio of intensity I_G /I_D could be used to determine defect concentration in CNTs [63]. The assignment of peaks used in this study is same as used by other authors [64, 65]. A sample of Raman spectrum of carbon nanotubes is shown in Figure 2.9. In our research, at least ten spots in each sample were analyzed and the averaged I_G /I_D were used to compare defects.

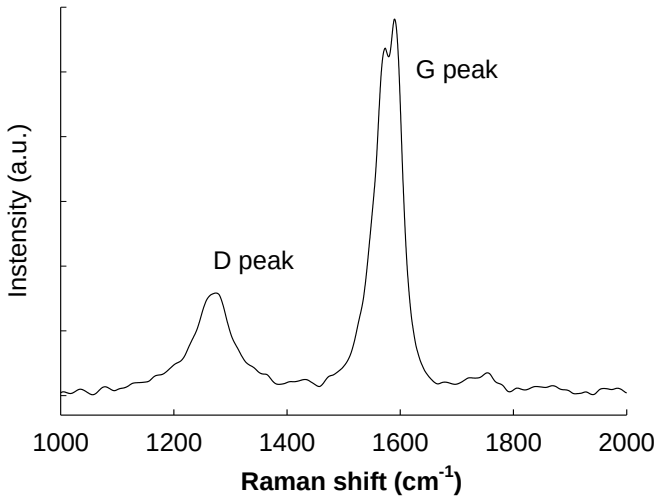

Figure 2.9 Raman spectrum

2.2.4 FT-IR

FTIR (Fourier Transform Infrared) spectroscopy is an analysis technique that provides information about the chemical bonding or molecular structure of materials, either organic or inorganic. The technique works on the fact that bonds and groups of bonds vibrate at characteristic frequencies. A molecule that is exposed to infrared rays absorbs infrared energy at frequencies which are characteristic to that molecule. During FT-IR analysis, a spot on the specimen is subjected to a modulated IR beam. The specimen's transmittance and reflectance of the infrared rays at different frequencies is translated into an IR absorption plot consisting of reverse peaks. The resulting FT-IR spectral pattern is then analyzed and matched with known signatures of identified materials.

In this research, a NICOLET 6700 Thermo FT-IR was applied to analyze surface

functional groups of carbon nanotube samples. The lasers emit continuous-wave laser energy at wavelength ranging from 532 nm to 785 nm. The same pellets made for Raman spectroscopy were used in this analysis. A blank KBr sample was used to clear out the influence of environment. Three spots in one sample were analyzed and each spot was scanned 32 times with resolution of 16. The assignments of peaks to surface functional groups are shown in Table 2.2, and an example of FT-IR spectrum is shown in Figure 2.10. The assignments of peaks are selected based on widely used methods. A list of papers which use FT-IR to analyze surface functional groups were attached in the Appendix II and their assignments of peaks to functional groups were close to ours [66-69].

Table 2.2 Assignments of infrared absorption peaks to functional groups

Absorption peaks(cm^{-1})	Assignments
3150-3400	Acetylenic C-H stretching
3030	Aromatic C-H stretching
2975-2925-2850	Asymmetric and symmetric C-H stretching of C-H3, C-H2 aliphatic groups, respectively
1730-1750	Carbonyl C=O stretching
1560-1595	Aromatic and alkene C=C stretching
1450-1380	Asymmetric CH3 and scissor CH2 deformations Symmetric CH3 deformation and cyclic CH2
1300-1000	C-O stretching
890-840-750	C-H bending out of the plane of condensed aromatic systems

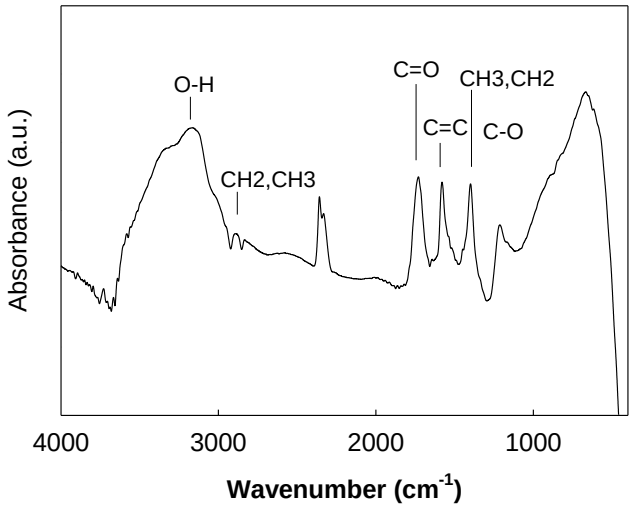

Figure 2.10 FI-IR spectrum of carbon nanotube

Figure 2.11 FI-IR and Raman spectroscopy located in SERF 702

2.3 Aging environment and timing

We aged samples in several conditions. Samples were first saved in ambient conditions for about 16 months and these samples were found to reach equilibrium status; then a part of these fully aged samples were moved to two other conditions, one with higher temperature (37°C) and another one with higher humidity (90%RH). These three aging conditions were introduced in the following sections.

2.3.1 Aging in the ambient condition

Samples were aged in open transparent glass bottles in this experiment and bottles were exposed to ambient lab conditions, which was about 20°C and 40-60% RH. Bottles were periodically shaken so that the entire samples had consistent exposure to the ambient conditions. Exposure to volatile organics and radiation, including sunlight, was carefully avoided during storage, transport and analyses.

A small amount of samples (~30 mg) were picked out for analysis, but the analyzed samples were not returned back in order to avoid cross-contamination. Samples were aged from September 2006 (the time when samples were manufactured) to September 2008. Totally, the aging process was lasted for about two years. Samples were analyzed periodically with about 5-month interval in 0-3 month, 7-10 month, 15-18month and 21-24 month.

2.3.2 Aging with 90% RH and ambient temperature

In this case, samples were saved in plastic bottles **(Fig. 2.12)**. A small flow of air was introduced into a water bottle and come out with high humidity. This humidified air flow was then inducted to a buffer to reduce pressure variation and was then inducted into the aging bottle. A hydrometer was used to measure relative humidity and temperature within the aging bottle; the flowrate was measured by a flow meter and controlled by a valve. The air flowrate was adjusted to maintain humidity. This aging temperature is just normal lab temperature. Samples were aged from March 2008 to November 2008 and were analyzed in the beginning (0 M), after 1 month (1M), 3 months (3 M) and 8 months (8 M).

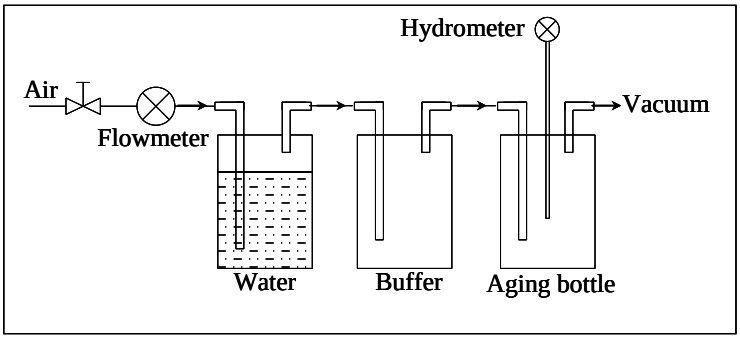

Figure 2.12 Aging with 90% RH in ambient temperature: Schematic of aging system (up) and experiment setup (down).

2.3.3 Aging in an oven with 37°C

Samples were saved in the transparent bottles, exposing to air. Bottles were located in an oven with controlled temperature of 37^{0}C **(Fig. 2.13)**. The oven exchanged inside air with ambient air. The humidity inside the oven was tested several times and found to be quite close to outside humidity, but the RH of inside air was lower than outside (because saturated vapor density increased with temperature). Samples were aged from March 2008 to April 2009 and were also analyzed in 0 M, 1M, 3M, 8M and 13M.

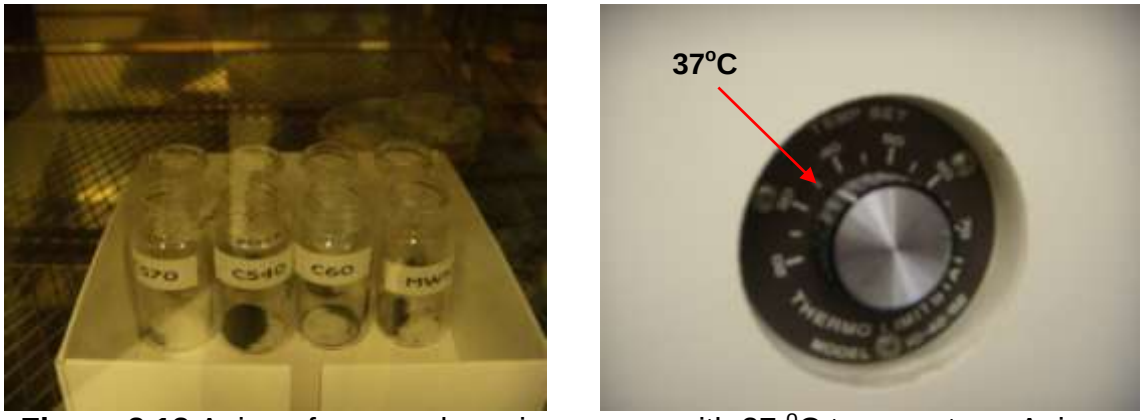

Figure 2.13 Aging of nanocarbons in an oven with 37 ^{o}C temperature. Aging samples inside of the oven (left) and oven temperature (right)

CHAPTER 3

RESULTS AND DISCUSSIONS

3.1 Aging in ambient conditions

In this study, four SWNTs (CS40, CS70, CS80 and BU90), one MWNTs and one fullerene (C60) were researched. Samples were exposed to ambient condition for 24 months from Sep. 2006 to Sep.2008 and their physicochemical properties were tracked by using N_2 adsorption technology, XPS, and Raman. New CS40, CS70 and CS80 samples were also purchased in Feb. 2009 and were analyzed to make a comparison with old SWNT samples. Physicochemical properties of new samples were supposed to be similar with old raw samples in the 0-3 month aging period.

3.1.1 Fluctuations of physical properties

Two main physical properties of nanocarbons, surface area and pore volume, were tracked in the 24-month aging research and the observed fluctuations clearly imply that aging changed the physical properties of nanocarbons **(Fig. 3.1, 3.2, 3.3)**. Samples were outgassed at temperature 100-600°C and then were analyzed by N_2 adsorption technologies in four periods with about 5 months interval (0-3 month, 7-10 month, 15-18 month and 21-24 month). The effect of outgassing at 100°C is widely believed to only be able to clear away weakly physisorbed gases and vapors while outgassing at higher temperatures (300-600 ^{o}C) may alter surface chemistry [19].

The BET surface area and total pore volume (P/P_0=0.90) of CS40 and BU90 were decreased with aging (the arrow in the **Fig. 3.1**). CS40 showed a big decrease in both surface area and pore volume during the first and second periods (0-3 month and 7-10 month). However, in the following two periods (15-18 month and 21-24 month), its surface area remained almost unchanged at 275 m^2/g; its pore volume kept decreasing until the third period and stabilized thereafter with the value of about 0.26 cm^3/g. Sample BU90, displayed a similar but much more smoothly trend in the aging period. It appeared that surface area and pore volume were decreased with a trend of approaching to equilibrium in the aging for both CS40 and BU90.

Micro surface area and micro pore volume (with pore width < 2 nm) of both samples were quite constant in the first and second periods, but were increased a little bit in the third period, and after then also remained almost unaffected in the fourth period.

The surface area and pore volume were increased by outgassing temperature; however, the increases were minimized with aging. In the first period, when outgassing temperature was increased from 100°C to 300°C, surface area and pore volume of sample CS40 and BU90 were increased obviously; when further aged to the second period, their surface area and pore volume were also enlarged, but were not as much as those obtained in the first period; in the third and fourth periods, the increase in surface area and pore volume were even less noticeable.

Another interesting observation was the comparison of CS70 and CS80 **(Fig. 3.2)**. These two samples were essential the same but were only purified differently. CS70 was

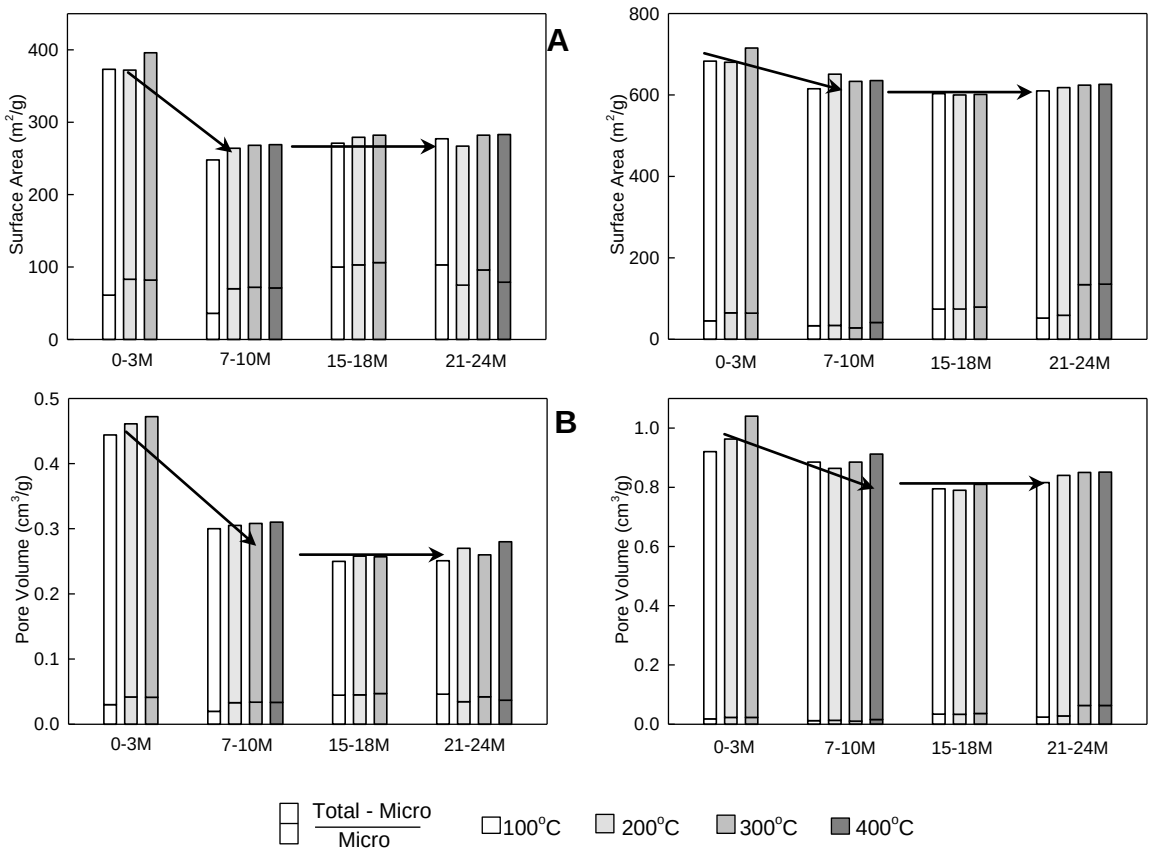

Figure 3.1 CS40 (left) and BU90 (right). A: BET Surface area and B: Total Pore volume (P/P_0=0.90).

Note: Total = BET surface area/ total pore volume; Micro = micro pore surface area/pore volume, same in the following figures.

purified by oxidation of air and left with low concentration of functional groups while CS80 was purified by oxidation of nitric acid and was left with high concentration of oxygen-contained functional groups **(Table 2.1)**. During the aging period, CS70 showed a very similar trend as CS40 and BU90, while CS80 had some differences. Firstly, it was clear that surface area/pore volume of CS70 were much higher than CS80; but when outgassing temperature was improved, surface area/pore volume of CS80 increased much more quickly CS70. In particular, when outgassing temperature changed from 200 ^{o}C to 300 ^{o}C, surface area and pore volume of CS80 rapidly increased by ~200% and ~50%, respectively. Secondly, unlike other three SWNT samples, surface area and pore volume of CS80 kept decreasing until the forth period, which suggested that it may need a little longer time to reach equilibrium. Reasons for these differences may be related to surface chemistry. CS80 had higher concentration of functional groups which could easily block tips and cavities of tubes which could make its surface area and pore volume much smaller than CS70; and when outgassed at higher temperature (200-300°C), more functional groups were removed or modified, thus created much larger surface area and pore volume. However, same as other three SWNTs, increases of CS80's surface area and pore volume by outgassing were also minimized with aging.

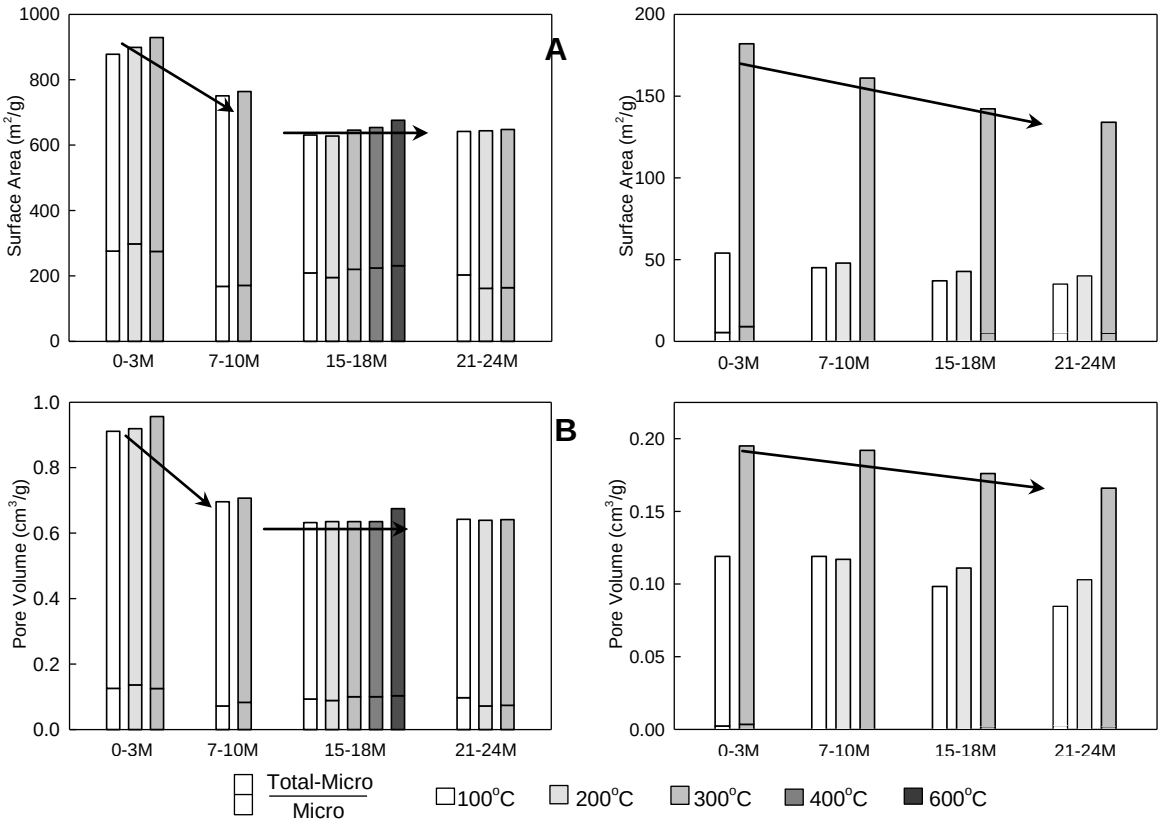

Figure 3.2 Sample CS70 (left) and CS80 (right). A: Surface area. B: Pore volume.

Physical properties of MWNT and C60 were tracked as well **(Fig. 3.3)**. The surface area and pore volume of MWNTs were exactly like BU90. Its surface area was reduced slowly but its pore volume was decreased sharply in the first and second periods; its physical properties were stabilized thereafter. Furthermore, little fluctuations of MWNTs were caused by higher temperature during the third and forth aging periods. The micro surface area and pore volume were increased with aging and also by outgassing (like CS40 and BU90). Fullerenes C60 also showed a decreasing trend (9.9 m^2/g decreased to 5.5 m^2/g in 15 months) in spite of the fact that these nanocarbons are essentially nonporous and, as a result, their surface area and pore volumes were significantly lower. It was also found that C60 tends to decompose at outgassing temperatures higher than

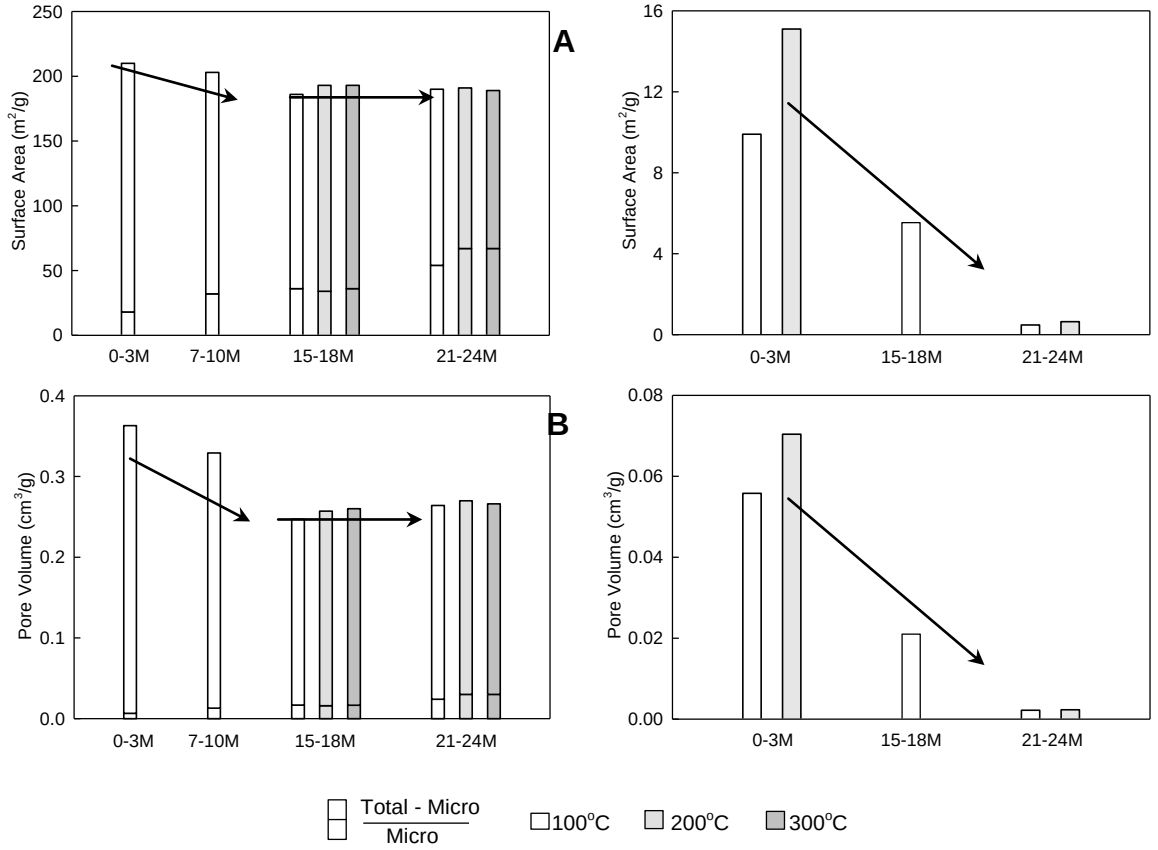

Figure 3.3 Sample MWNTs (left) and C60 (right). A: Surface area and B: Pore volume.

200 ^{o}C. The results of C60 showed that this aging profile of physical parameters was not unique to carbon nanotubes, but would be applicable for all nanocarbons.

In all, based on the physical properties of six samples, we could make several meaningful conclusions: First, aging in the ambient conditions for a long period of time would reduce surface area and pore volume of nanocarbons (CNTs and fullerenes), which could lead to decrease of adsorption capacity. Second, surface area and pore volume of nanocarbons kept constant after aging for 15-18 month which indicted that nanocarbons could reach a more structurally stable state after aging in ambient condition. Third, increase of surface area and pore volume caused by heat treatment could be minimized with aging; since higher temperatures reduce the concentration of surface oxides, a reasonable explanation for this phenomenon would be that aging also lowers the total surface oxygen on nanocarbons. This was confirmed by spectroscopic characterization of samples and is presented in the following section.

3.1.2 Fluctuations of chemical properties

Chemical properties of nanocarbons were presented by elemental contents, surface functional groups and structural defects. The contents of two main elements within nanocarbons, oxygen (O) and carbon (C), were analyzed by XPS survey scan in the 0-3M, 12-15M and 21-24M; three major surface function groups: -C-O, -C=O and –COOH were obtained by XPS carbon C1s scan at the same time; and defects of nanocarbons were measured by Raman spectroscopy. The XPS C1s scan analysis in the 0-3M used 89eV passing energy while in 12-15M and 21-24M applied 25eV passing

energy for carbon C1s scan, therefore in order to verify passing energy independence, additional CS40, CS70, and CS80 samples were purchased in 2009 as representatives of 0-3M aged old samples. These samples (referred to as 0-3M (new)) were analyzed by the same instrument as the one used for old samples (25 eV passing energies).

Oxygen contents of the six nanocarbons and carbon C1s spectrum of CS70 are presented in Figure 3.4. A visible decrease of oxygen in CS70 (old sample) was observed (Fig. 3.4 A); and the bar chart in Fig. 3.4B clearly showed that oxygen contents of old samples were steadily decreased after aging for 12-15 months but only very slightly decrease were observed during 12-24 month.

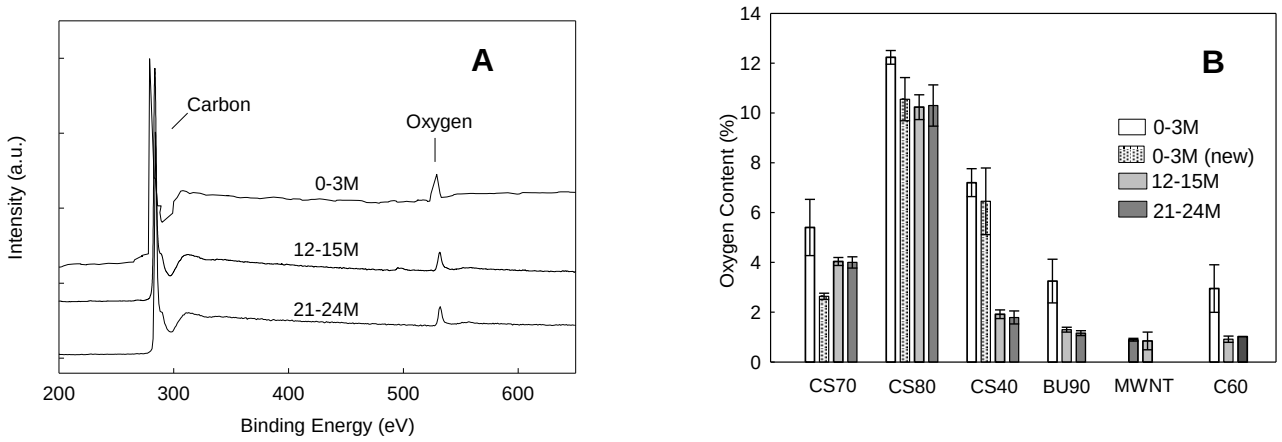

Figure 3.4 Results of X-ray Photoelectron Spectroscopy: (A) survey spectra of CS70 and (B) summary of oxygen contents in nanocarbons. The error bars represent one standard deviation based on 3 replicates.

Sample CS70 exhibited a decrease from 5.2% to 4.0% oxygen with 24 months of aging. Sample CS80 had the greatest amount of oxygen (12.3%) of all samples (consistent with the manufacturer provided information) which then reduced to 10.5% with 24 months of aging. This value is significantly higher in comparison to other samples which explains why outgassing conditions can continue to increase its surface area and pore volumes. CS40 exhibited a sharp decrease from 7.1% to 2.0% oxygen with 15 months and 1.9% oxygen with 24 months of aging. It should be noted that this is an untreated as-produced sample and, therefore, it was expected to have low surface oxygen from the beginning. Surprisingly the high oxygen value (7.1%) in a 0-3 month aged sample was confirmed from the analysis of the newly purchased sample (6.2% of the 0-3M (new) CS40 bar in figure). It should also be noted that the surface oxygen is low in an aged sample CS40 (1.9%) and is more consistent with the levels that are expected for as-produced samples. BU90 also showed a similar pattern. This sample had 3.0% oxygen when tested within 3 months of aging but it was found to have reduced to 1.6% at 15 months and 1.5% at 24 months of aging. MWNTs had the lowest surface oxygen (< 1 %) that was anomalous in comparison to other nanocarbon samples but consistent with the observation that its surface area and pore volumes were also the least affected by aging. C60 exhibited a decrease from 3.5% to 0.8% oxygen with 24 months of aging. The valuable observation here is that the most significant decrease in sample's oxygen contents occurred during the same time period that the greatest decrease in surface area and pore volumes was observed (i.e., within 15 months).

The new CS40 and CS80 had slightly lower oxygen contents than 0-3 month aged

old samples but still higher than 12-15 month and 21-24 month aged samples, and the highest values of new samples were quite close to the 0-3 month aged old samples. Surprisingly, % oxygen of CS70 was much lower than the 0-3 month old sample and even lower than 12-15 month and 21-24 month aged samples which indicted that the manufacturing/purification process may have changed for CS70.

The oxygen content trends were not only consistent with surface area and pore volume, but also supported the physical changes. It explains the differences in physical properties between CS70 and CS80: CS80 had much higher concentration of oxygen contained functional groups which reduced surface area and pore volume; also, since a part of oxygen were rejected from nanocarbons, therefore the increase of surface area and pore volume by heating were minimized; and the most important, % oxygen was unaffected during 15-24 month which strengthen the point that samples had been fully aged, which leaded to the same trend of physical properties. Therefore, we conclude that it was the fluctuation of chemical properties that lead to physical properties variation in aging period.

Contents of -C-O, and -C=O and -COOH extracted from C1s scan spectrums were further investigated. Since the Carbon C1s analysis used a different passing energy in 0-3M (89eV) and 12-15M, 21-24M (25eV), and resolution of an XPS C1s scan are varied with passing energy, therefore, we only report results in 12-15M and 21-24M here. The new CS40, CS70 and CS80 samples were also tested with 25 eV pass energy, so their results were compared with old samples (**Fig 3.5**). Deconvolution results of old BU90, MWNT and C60 samples were presented in Table 3.1.

The figures clearly showed that functional groups of CNTs were decreased in aging. CS70 had a steady decrease in its -C-O and -COOH concentrations when compared 0-3M(new) with 12-15M results, and was continuing decreased slightly until 21-24M. CS80 lost some -COOH from 5.2% in 0-3M to 4.7% in 12-15M, and further reduced to 4.5% in 21-24M; the sum of three functional groups of CS80 demonstrated that this sample was unstable and would keep decreasing in its oxygen content. Three oxygen contained functional groups of CS40 were decreased quite steadily from 0-3M(new) (totally 20.1%) to 12-15M (totally 16.7%); but almost remained unchanged thereafter at 16.0% when aged up to 24 months, in particular, its -C=O, and -COOH concentrations were same as they were in 12-15M. The decreasing trends here were same as shown in XPS survey scan results, therefore, it could be said that oxygen was rejected from the surface of nanocarbons in aging, but have a trend of approaching to equilibrium status.

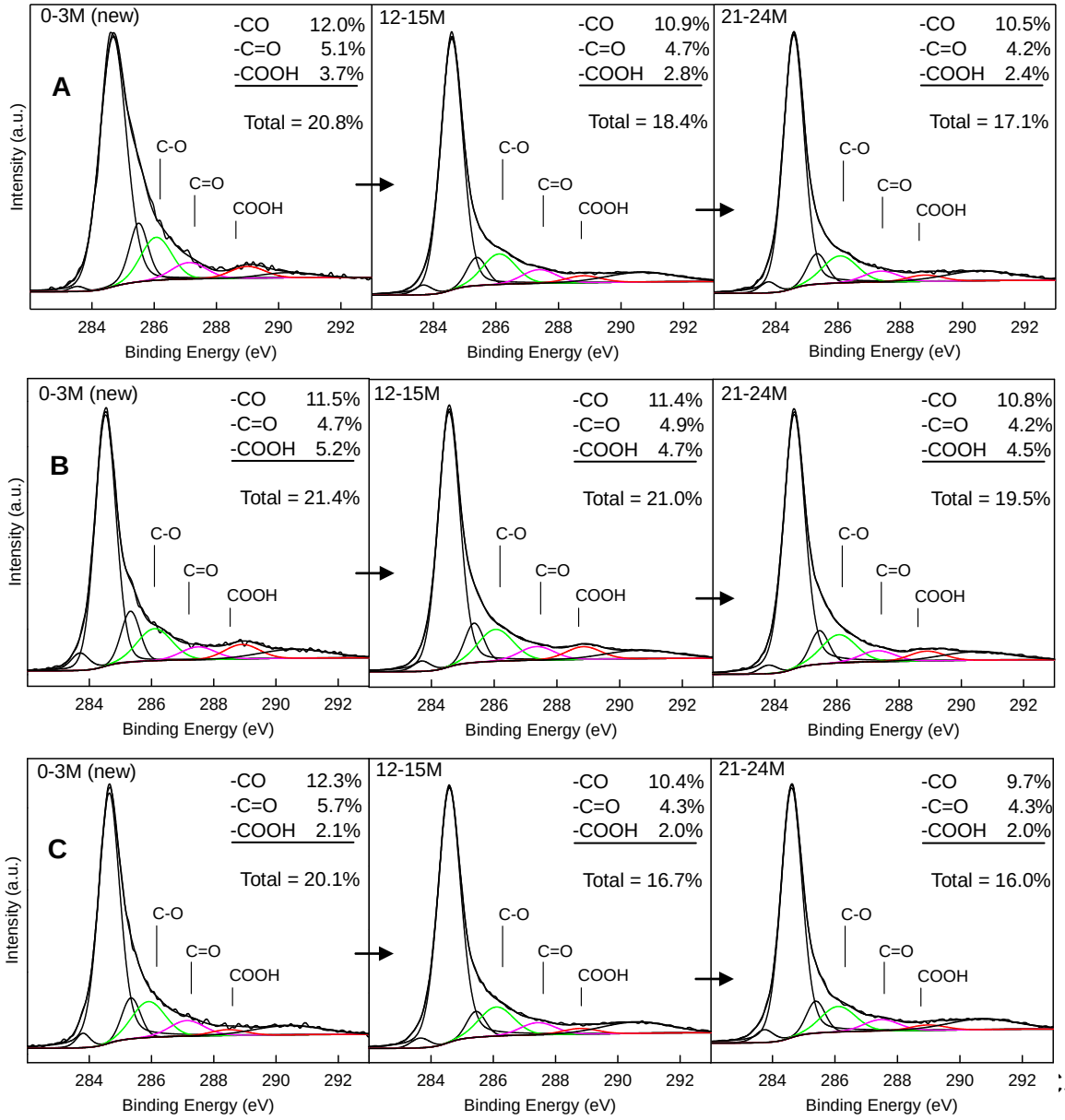

:S40 (C).

0-3 (new) samples were just manufactured and purchased in Feb.2009.

In the stable status, -C-O was demonstrated to be the main functional group in all three samples, which accounted for 50-70% of total oxygen contained functional group. Another interesting observation is that in CS40, CS70, BU90 and MWNT **(Table 3.2)**, concentration of -C=O is higher than -COOH, but in CS80, conc. of –C=O and -COOH were very similar. Comparison of CS70 and CS80 further tells that highly functionalized sample CS80 has roughly same conc. of -C-O, and -C=O as CS70, but had much higher concentration of -COOH. This observation made sense in explaining the differences in physical properties between CS70 and CS80. The sum of three functional groups (C(O)) followed the same trend as XPS survey scan, which is CS80 > CS70 > CS40 > BU90 > MWNT > C60. However, the conc. differences are not as obvious as they are in survey scan, it seems that deconvolution of C1s scan had a much narrower window than XPS survey scan.

Table 3.1 Results of functional groups obtained from deconvolution

Sample	Aging Month	-C-O (%)	-C=O (%)	-COOH (%)	Total (%)
BU90	14-16	9.99±0.053	4.29±0.086	2.16±0.086	16.44±0.119
	24-27	10.26±0.203	3.93±0.073	2.19±0.122	16.37±0.296
	Avg.	10.13	4.11	2.18	16.41
MWNT	14-16	9.49±0.106	3.85±0.100	1.62±0.027	14.96±0.141
	24-27	9.11±0.000	3.73±0.000	1.55±0.000	14.39±0.000
	Avg.	9.30	3.79	1.58	14.68
C60	14-16	5.73±0.722	1.98±0.280	2.00±0.181	9.70±0.820
	24-27	6.16±0.420	0.80±0.110	2.40±0.070	9.25±0.245
	Avg.	5.95	1.39	2.20	9.48

* Values obtained are based on peak area of carbon C1s scan deconvolution.

The XPS results were very interesting. In contrast to previous studies of activated carbon and carbon membrane which found that carbon gained oxygen after aging, this research demonstrated that % oxygen in nanocarbons were decreased and the results were confirmed by both XPS survey scan and carbon C1s scan. Therefore, our observations indicted that the nanometric scale carbon materials may have a different aging process from bulk carbon materials. Both our research and previous research show that equilibrium status would be achieved if sufficiently aged.

Broadly speaking, aging of carbon is highly depended on aging environment. High humidity, presence of oxidized pollutants such as ozone with strong sunlight would build oxygen to carbons [22, 48]. In our research, however, aging environment was set as general lab condition, which was about 40-60% relative humidity, and about 20°C temperature, no strong sunlight or UV light exposure, and oxidized gases were also carefully prevented. Therefore, it seems that nanocarbons rejected oxygen "automatically" in the ambient condition. In order to maintain electroneutrality, this also suggests that the covalently bonded sp^3 carbon of an oxygen-losing functional group could bond with a similar carbon of a nearby functional group. These defective sites have been found to be more reactive than graphite sites, and functional groups are more likely to attach to defective carbon atoms [70-73]. If such a structural-rearrangement were to take place then aging should suppress the sp^3 carbon defect-site concentration and enhance the concentration of sp^2 carbon of the pristine matrix. This phenomenon should then be observable from tracking the I_D/I_G ratio in the Raman spectra of samples,

particularly SWNTs.

We characterized newly purchased samples (as representative of 0 to 3 month of age) and the 21-24M aged CS70, CS80 and CS40 by Raman (**Fig. 3.6A**) and calculated their I_D/I_G ratios (**Fig. 3.6B**). It was found that for CS80 and CS40 this ratio was significantly lower in the aged sample. Furthermore, the decrease in CS40 (0.47 to 0.21 with 24 months aging) was far greater than that in CS80 (0.63 to 0.57 with 24 months aging). CS70, however, showed an opposite trend which is most likely due to manufacturing changes in the past 24 months. In all three samples the trends in I_D/I_G ratios were surprisingly similar to the trends in total oxygen contents (**Fig 3.4**). This strengthens the concept of a relation between surface-oxygen and structural-defect concentrations evolving with aging.

Combining the results of three types of analysis, it is interesting to see that surface area, pore volume, surface oxygen and structural defects of these nanocarbons had very similar trends during the aging process. These observations of physicochemical properties of carbon nanotubes help understand the aging effect. We deduce that carbon nanotubes are meta-stable materials (i.e., they are in a pseudo-thermodynamic equilibrium) and interaction with pristine ambient conditions makes them more thermodynamically stable. Therefore, their physicochemical properties can be characterized with reliability only after the samples have sufficiently aged. It can also be stated that the nanocarbon's ability to reject surface oxygen and "repair" itself is the

mechanism by which a more stable configuration is achieved with aging. As observed here, SWNTs appear to be more meta-stable than MWNTs. This is most likely due to the fact that carbon atoms in SWNTs are present as surface-atoms only, which brings out the 1-D electronic properties thus differentiating nanomaterials from bulk materials. The thermodynamically stable state is obviously related to the ambient conditions, notably humidity, oxidizing air pollutants and radiation which are known to build oxygen on most common carbons. Their effects on nanocarbons were examined in the following chapters.

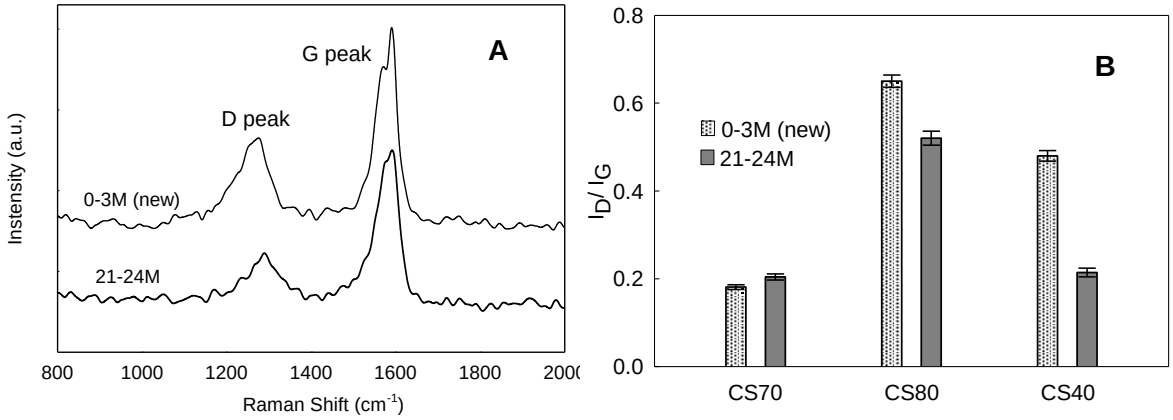

Figure 3.6 Results of Raman Spectroscopy: (A) spectra of CS80 and (B) measured Id/Ig in SWNTs under aging. The error bar represents one standard deviation based on 8~10 replicates.

3.1.3 Summary

In this study, the aging effects of nanocarbons in ambient conditions for 24 months were researched. Physicochemical properties of nanocarbons were analyzed by three instruments. The study showed that aging of nanocarbons was quite different from bulk carbon materials. The surface area, pore volume and structural defects of nanocarbons were decreased but could reach equilibrium status in 15-18 month. The oxygen was rejected from nanocarbons and the concentrations of surface functional groups were reduced in the beginning months, but also could be fully aged within 9-12 months. This research demonstrated that it was the chemical properties of nanocarbons that caused the fluctuation of physical properties. We conclude that nanocarbons are meta-stable materials, and that their aging in ambient conditions has an unexpected effect whereby oxygen leaves their surface, at the same time the structure repairs itself and they become more thermodynamically stable with fixed properties.

3.2 Aging with 90% RH

Humidity is considered as an important factor in aging of carbon which is known to be able to promote chemisorption of oxygen in the air to carbon surface [48, 74-76]. Thus, it is important to study aging of nanocarbons in the environment with higher RH. In present paper, RH was raised to 90% at room temperature. Five samples (these samples had aged in ambient conditions), including four SWNTs (CS70, CS80, BU80, and BU90) and one MWNTs, were aged in a chamber in which RH was controlled **(Fig. 2.12)**. These samples were aged from March 2008 to December 2008, totally 8 months; the raw samples (0M, also was the 17th month from Sep. 2006) were analyzed, and samples were also analyzed in 1 month (1M), 3 months (3M) and 8 months (8M) by N_2 adsorption technology, XPS, Raman, FT-IR.

3.3.1 Fluctuations of physical properties

Surface area and pore volume were analyzed by N_2 adsorption technology. The results showed that BET surface area and total pore volume (P/P_0) were decreased in this condition and have a trend of approaching to equilibrium **(Fig. 3.7)**. It seems that sample BU90 and MWNTs were closing to stable statuses in 3 to 8 months (blue arrow in the figure), while CS70, CS80 and BU80 kept decreasing in whole 8 months (red arrow in the figure). These observations were similar with those in ambient conditions **(Fig. 3.1)**, which indicted that humidity may play a role of “enhancing” aging of nanocarbons.

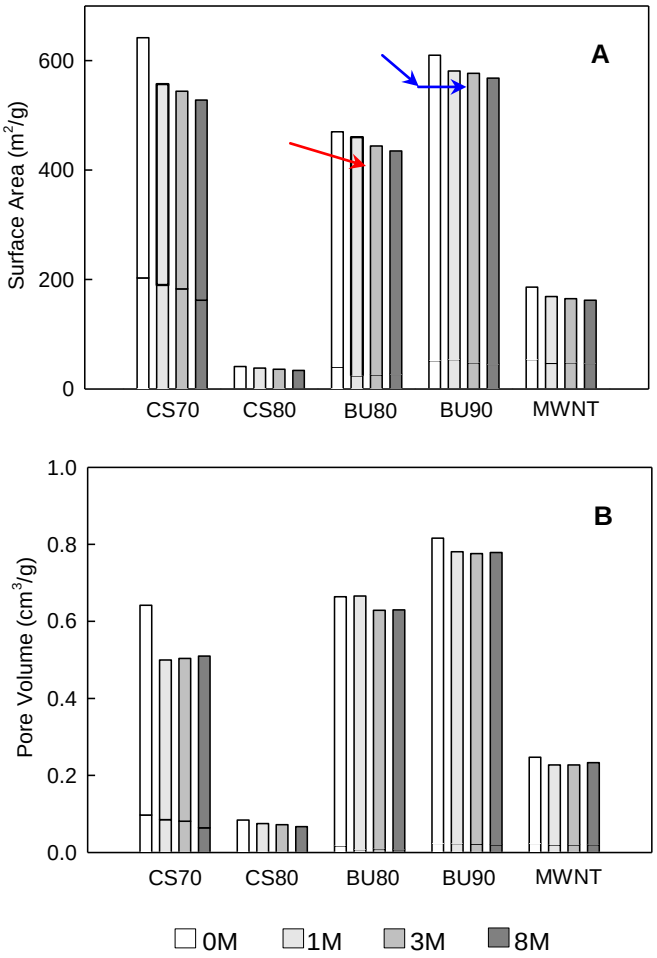

Figure 3.7 Aging of nanocarbons with 90% RH for 8 months. A: Surface area; B: pore volume.

3.3.2 Fluctuations of surface chemistry

Oxygen contents of nanocarbons were analyzed to investigate surface chemistry by XPS survey scan. The results are shown in Figure 3.8. Oxygen content of CS70 was increased steadily with aging in 0-8 month (left blue arrow in the figure). % oxygen of CS80 also increased slowly in 8 months (right blue arrow in the figure). Both BU80 and BU90 had an obvious increase in 0-1 month, though there were no data available in 3-8 months. MWNTs also obtained oxygen. The increase of oxygen content is probably because high relative humidity promoted oxygen/carbon reaction and produced more functional groups.

The role of water vapor as a promoter of chemisorption of oxygen to carbon was observer by several other groups [48, 74-77], though they come up with different explanations for the promoting process. Billinge et al. aged activated carbon with atmospheric pressure, ambient temperature (21 ± 2^{0}C) and RH from ambient condition to 98% for 56 days. They found that surface area of activated carbon was reduced but oxygen content was increased when RH was raised from below 40% to 80% and almost stable thereafter. They concluded that with the presence of water vapor, the mineral matter in the surface of activated carbon play a catalytic role in the oxygen/carbon oxidation process [75]. Also, according to Adams et al., the results of Billinge et al. are consistent with chemisorption of oxygen and/or water from humid air [76]. However, Petit and Bahaddi researched two systems: water vapor/oxidized activated carbon (in which free oxygen in excess has been removed) and water vapor/un-oxidized or degassed

activated carbon and found that the CO_2 evolution in the latter system was much less than former system, from where they concluded that at room temperature, hydrolysis reaction is able to replace pyrolysis (which works only at higher temperature) for the production of reactive species allowing the oxidation process to be continued, which explained the promoter role of water vapor [48]. Pierces et al. also proposed the oxidation reaction at ambient temperatures in the presence of air and water, which he thought was: $C + H_2O = CO_2 + H_2 + C - Ocomplex$ [78, 79]. The argument between these authors is: whether water reacts with carbon directly or water is only a kind of catalyst. The present work is not going to solve this argument, but to confirm that stabilized nanocarbons could obtain more oxygen with high relative humidity which is similar as other bulk carbon materials (activated carbon, coal, et al.).

This conclusion is further evidenced by the deconvolution of carbon C1s scan

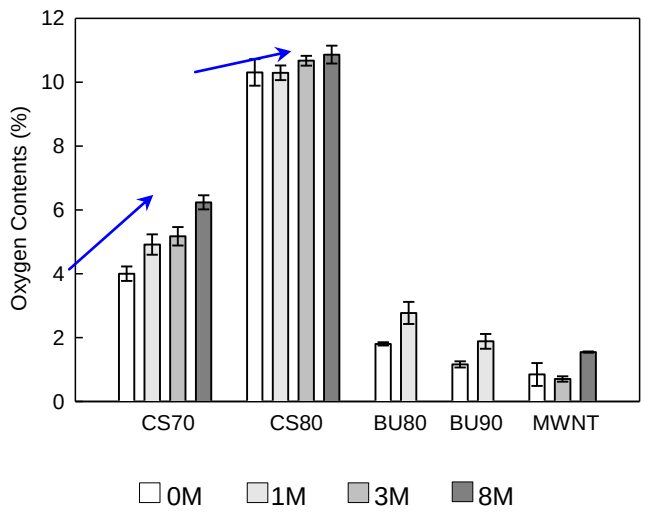

Figure 3.8 Oxygen content of nanocarbons in aging with 90% RH for 8 months

spectrums **(Fig. 3.9, Fig. 3.10)**. The sum of three functional groups (-C-O, -C=O, -COOH) in both CS70 and CS80 were increased with aging. With regarding to CS70, -C=O was the major increased specie in the 0-1M; but -COOH was strongly enhanced from 2.19% to 2.47% in 1-3 months, and was further increased to 2.82% in 3-8 months. Therefore, totally, -COOH offered highest oxygen increase in CS70, which accounted for ~70%. With regarding to CS80, the three functional groups were increased in 0-1M, in particular, -C=O was raised from 4.62% to 5.14%. Functional groups were still increasing in 1-3M; and in 3-8M, -C-O jumped from 11.15% to 11.67%, but -C=O, -COOH were almost unchanged. In whole 8 months, CS80 obtained much more -C-O and -C=O than -COOH. This result was exactly opposite to CS70. But given the initial CS80 contained much more –COOH than CS70 but had almost same –C-O, -C=O as CS70, the result was reasonable. The deconvolution also demonstrates that in the beginning step (0-1M), -C=O was the main increasing specie in both CS70 and CS80 which indicates that chemisorption of oxygen to carbon maybe the dominant process.

Functional groups were also analyzed by FT-IR **(Fig. 3.11)**. -C-O, -C=O, O-H, C=C, and C-H were assigned according to a widely accepted method **(Table 2.2)**. Generally, FT-IR was used for quantifying chemical species which could be determined by the location of peaks. In this study, we observed that the locations and numbers of peaks were not changed after aging which indicated that functional groups were neither totally removed nor any new type of species were created. Concentration of functional groups could be compared by the relative peak area. Take CS80 for example, it seems that the relative peak area of -C-O in the third month was higher than it was in the 0M, which show that the -C-O may be enhanced. This is consistent with XPS deconvolution result.

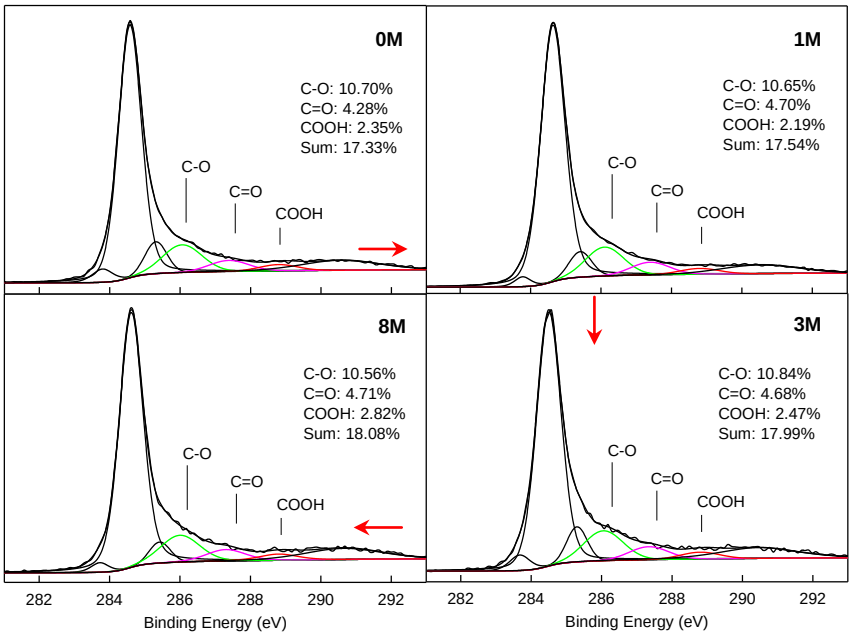

Figure 3.9 Deconvolution of CS70 C1s scan in aging with 90% RH for 8 months.

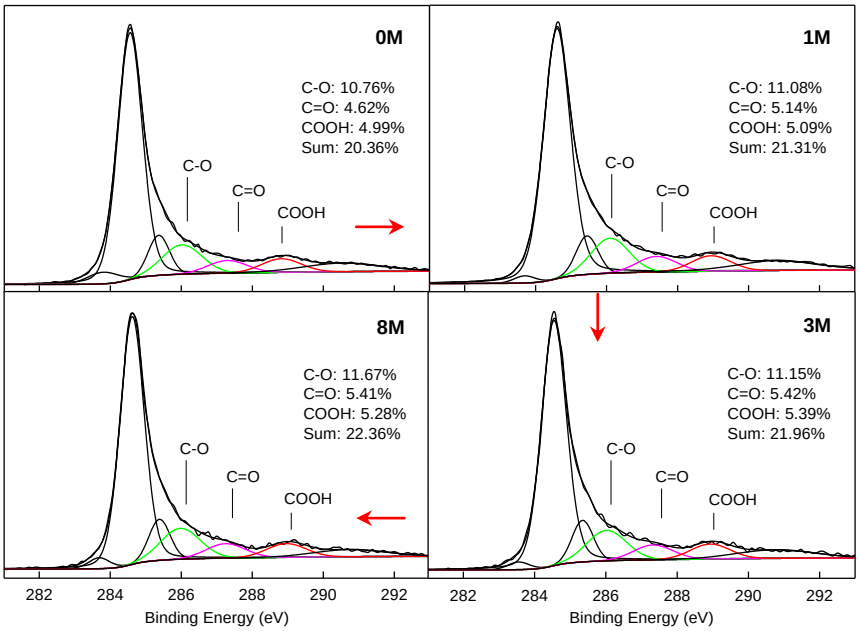

Figure 3.10 Deconvolution of CS80 C1s scan in aging with 90% RH for 8 months.

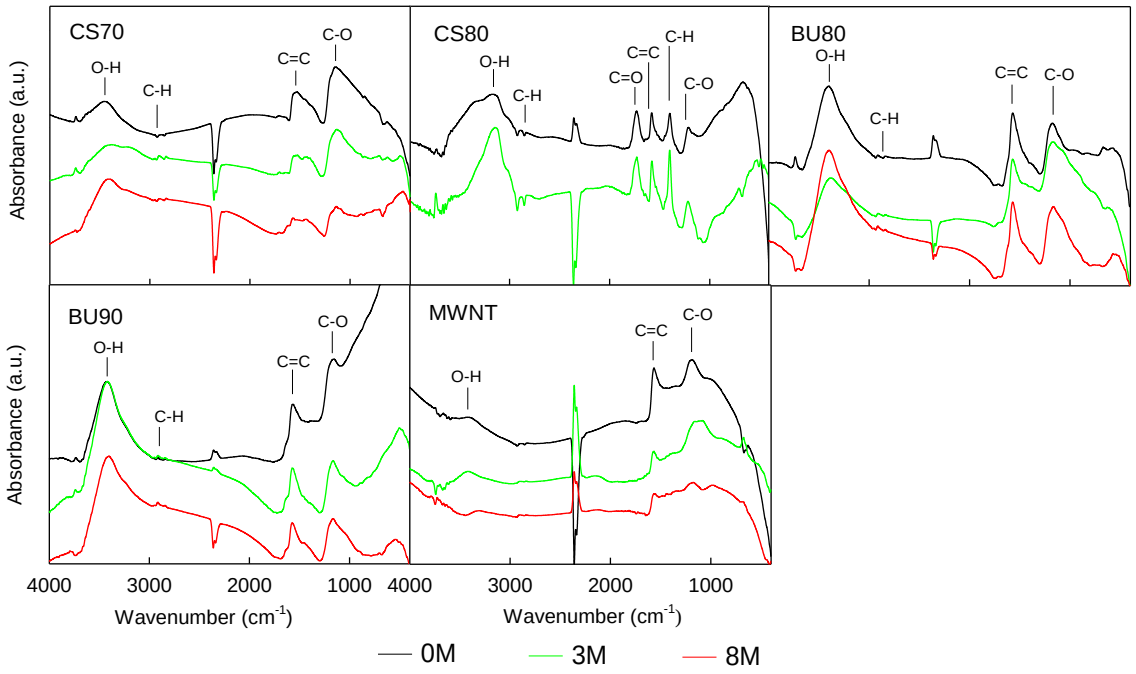

Figure 3.11 Surface chemistry of nanocarbons: aging with 90% RH for 8 months

Aging in ambient condition showed that oxygen was rejected and the newly manufactured nanocarbons become more stable in 15-18 months; while in 90%RH, nanocarbons obtained oxygen from air/water. Therefore, it means that the self-repair of nanocarbons and chemisorption of oxygen/water were in effort together in aging. In ambient condition, newly produced nanocarbons were metastable materials and reject oxygen; at 90%RH, high humidity somehow enhanced chemisorption of oxygen and/or water thus nanocarbons obtained more oxygen than rejection. Also in the ambient condition, the trend of surface area/ pore volume was same as structural defects; in 90%RH, the surface area /pore volume was further reduced, and we also found the defects were either decreased or unchanged **(Fig. 3.12)**. This confirms that the self-repair of nanocarbons still played an important role in this condition, though more carbon atoms were oxidized. Also, it forced us to conclude that most of the oxidation should be happened to defect sites which were not occupied by functional groups before.

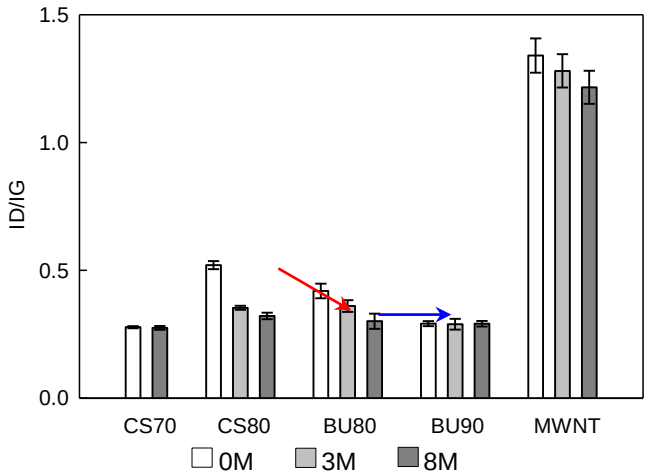

Figure 3.12 Defects of nanocarbons in aging with 90% RH for 8 months.

3.3.3 Summary

Nanocarbons were saved in 90% RH and ambient room temperature for 8 months. Surface area/ pore volume, and structural defects of nanocarbons were reduced and may have a trend of approaching to stable conditions. High RH also promoted chemisorption of oxygen and/or water in the air to nanocarbons which lead to the increase of % oxygen. It is possible that chemisorption of oxygen to carbon atoms was the dominant process in the beginning aging process. The changing concentration of functional groups was also evidenced by FT-IR. The study showed that self-repair of nanocarbons and chemisorption of oxygen and/or water to nanocarbons would be in working together in the 8-month aging process. Given the decrease of defects, we conclude that previous unoccupied defect sites should be the location where carbon atoms were oxidized in this condition.

3.2 Aging at 37 ^{o}C

Environment with 37°C temperature was selected as the third aging condition to compare with the ambient condition in which temperature is about 20°C. In most parts of this country, 37°C is a high temperature; therefore, it is meaningful to know how nanocarbons would be aged at this temperature. Small amounts (60-100 mg) of 16-17 months aged nanocarbons (in ambient condition) were moved to an oven and the temperature of oven was set at 37°C. The humidity inside of the oven was tested several times and was known to be about 15-20%RH, and the actual humidity was a little bit lower than outside ambient lab condition **(Table 3.2)**. The 13-month aging research was conducted from March 2008 to April 2009. Five nanocarbons were studied, including four SWNTs (CS70, CS80, BU80 and BU90) and one MWNT. We use N_2 adsorption technology, XPS, Raman and FT-IR to analyze these samples.

3.2 Records of temperature and humidity in aging oven and lab

Lab condition			**Aging environment**		
Temp. (^{o}C)	**RH** (%)	**Actual humidity** (g/m^3)	**Temp.** (^{o}C)	**RH** (%)	**Actual humidity** (g/m^3)
19.7	41	6.95	36.8	14.8	6.48
22.9	44.0	9.00	36.5	16.8	7.21
21.7	46	8.78	36.0	18.0	7.53
21.5	41	7.73	35.9	17.0	7.08
23.4	44	9.23	36.0	21.0	8.78

3.2.1 Fluctuations of physical properties

The changes of surface area and pore volume were found to be interesting **(Fig. 3.13)**. All five nanocarbons were decreased in the beginning 1-3 months, in particular, CS70 and BU80 were decreased quite a lot; however, surface area and pore volume of nanocarbons were found to be increased later in 3-13 months; the changing of pore volume appeared to be even stronger than surface area. The changes of micro surface area and micro pore volume were also similar. The big fluctuations of surface area and pore volume within 13 months showed that aging with 37°C could strongly modify physical properties of nanocarbons. Furthermore, the increase of temperature may also be able to speed aging.

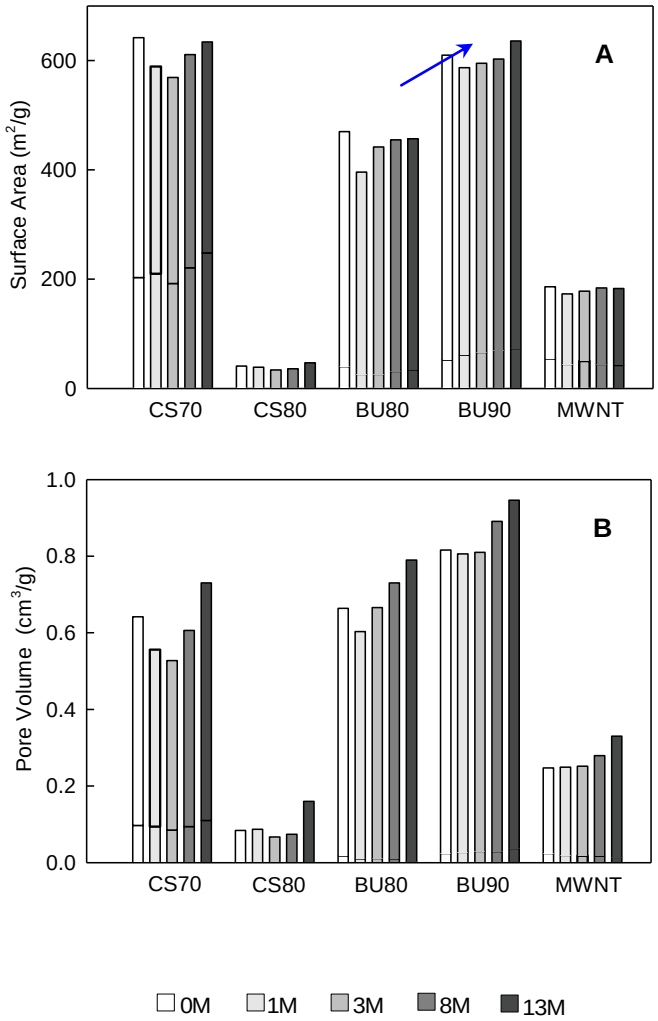

Figure 3.13 Aging of nanocarbons with 37°C for 13 months. **A**: Surface area; **B**: Pore volume.

3.2.2 Fluctuations of surface chemistry

Oxygen contents (0-8 months) of nanocarbons were analyzed. The results are shown in the Figure 3.14. % oxygen of CS70 and BU80 was quite constant; CS80 and MWNTs slightly decreased oxygen; while % oxygen of BU90 was increased a little bit. The missing of % oxygen of BU80 and BU90 in 3M and 8M make it difficult to draw a clear conclusion. However, since CS80 contained much more functional groups than other four samples, therefore, it could be less affected by experiment error, thus may offer a trend for nanocarbons in this condition. Compared with ambient condition, the temperature is increased but humidity was reduced, therefore, we can deduce that the decrease of oxygen could be due to the low humidity. There are also two other explanations in the literatures. Garcia-Perez et al. thought that there may be more intense interactions among adsorbed water with higher temperature (50°C) which could cause reduction of sorption capacity when they researched on water adsorption to lemon peel[80]; A more traditional idea is that carbon could be oxidized by oxygen in the air and/or attached oxygen contained functional groups to produce gas-phase CO_2/CO, and when temperature is increased, the ratio of O_2(abs)/CO_2 would be decreased which make % oxygen smaller [77]. Furthermore, it should not be ignored that when temperature is increased, self-repair of nanocarbons is also supposed to be speeded, though we still not sure that this reaction is endothermic or exothermic.

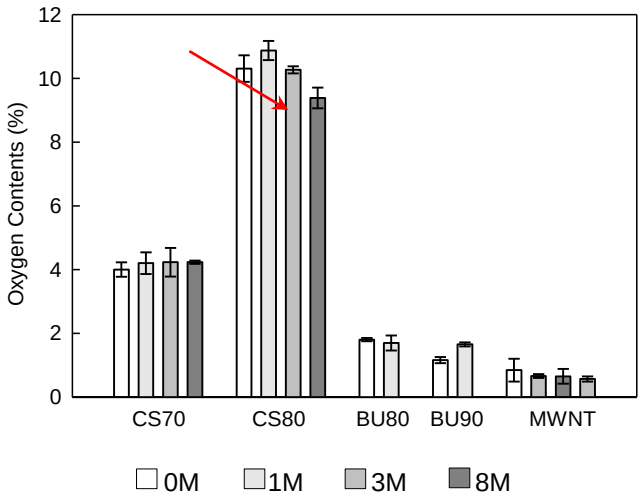

Figure 3.14 Oxygen contents of nanocarbons in aging with 37°C for 8 months. The error bar represents one standard deviation based on 3 replicates.

The self-repair effect was confirmed by Raman analysis **(Fig. 3.15)**. It is interesting to see that defects in CS70 and CS80 were decreased quite strongly in 0-3 months, which may be able to explain the decrease in surface area and pore volume in the beginning months. Defects of BU80, BU90 and MWNT were quite constant in 13 months. The results were consistent with aging in ambient condition (17-24M). Because CS80 and CS70 contained much more functional groups thus could not be fully aged when aging environment was changed from ambient condition to 37°C, therefore, metastable nanocarbons were continuing to repair defects and reject oxygen which could contribute to the decrease of % oxygen observed in XPS survey scan. The chemical properties of BU80, BU90 and MWNT were quite stable after 16 months of aging in ambient condition and were not affected strongly by increasing of aging temperature.

The changing of surface chemistry in CS80 was further analyzed by deconvolution

(Fig. 3.16). The sum of three functional groups followed the same trend as survey scan results. Compared the initial composition to the final status, we can see that total three functional groups decreased from 20.36% to 19.95% (overall,-0.41%); while concentration of –COOH decreased from 4.99% to 4.69% (-0.30%). Given the fact that in 90%RH, -COOH was the main increase for CS70; therefore, besides the oxygen rejection by self-repair effect of nanocarbons, it is possible that the decrease of oxygen here is also due to the lower humidity.

FT-IR results added more evidences for changing of surface chemistry **(Fig. 3.17)**. It clearly showed that in all five samples, the ratio of peak areas were quite different in three aging periods. For example, the peak area of -C=O, -C-H in CS80 were quite close to each other in 0M; however, the peak area of -C=O became much smaller than that of -C-H in the third month and the 8th month. The results could be caused by: (1) –C=O was decreased but -C-H didn't change, or (2) -C-H was increased but -C=O didn't change, or (3) both –C=O, and -C-H were changed. Therefore, it was for sure that at least one kind of functional groups were altered and -C=O became less dominant than C-H after aging. In some degree, this conclusion could support the decrease of -C=O, -COOH from XPS deconvolution **(Fig. 3.16)**.

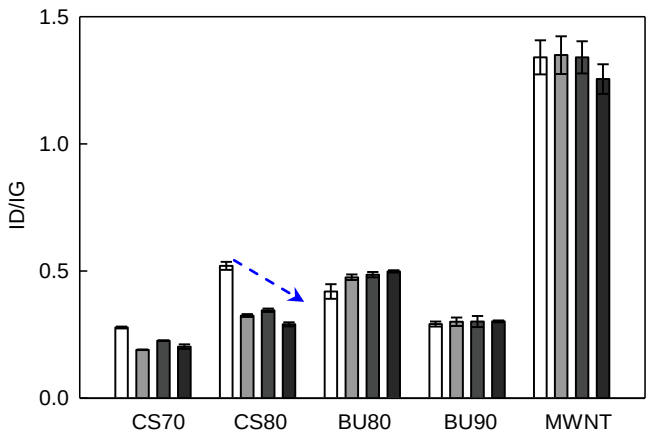

Figure 3.15 Defects of nanocarbons in aging with 37 ^{o}C for 13 months. The error bar represents one standard deviation based on 8 replicates.

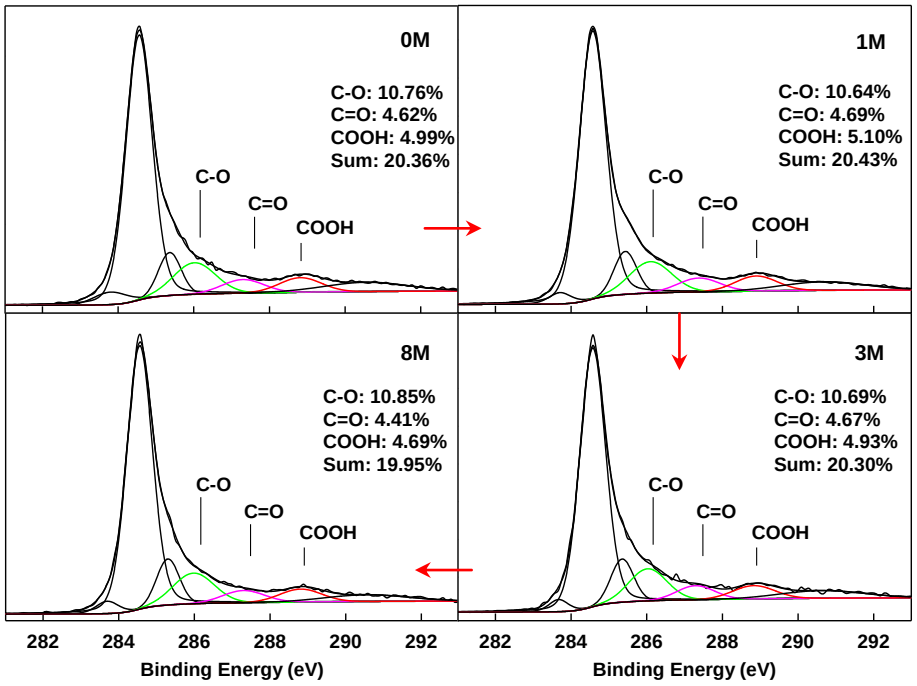

Figure 3.16 Deconvolution of CS80 XPS C1s scan in aging with 37°C for 8-month.

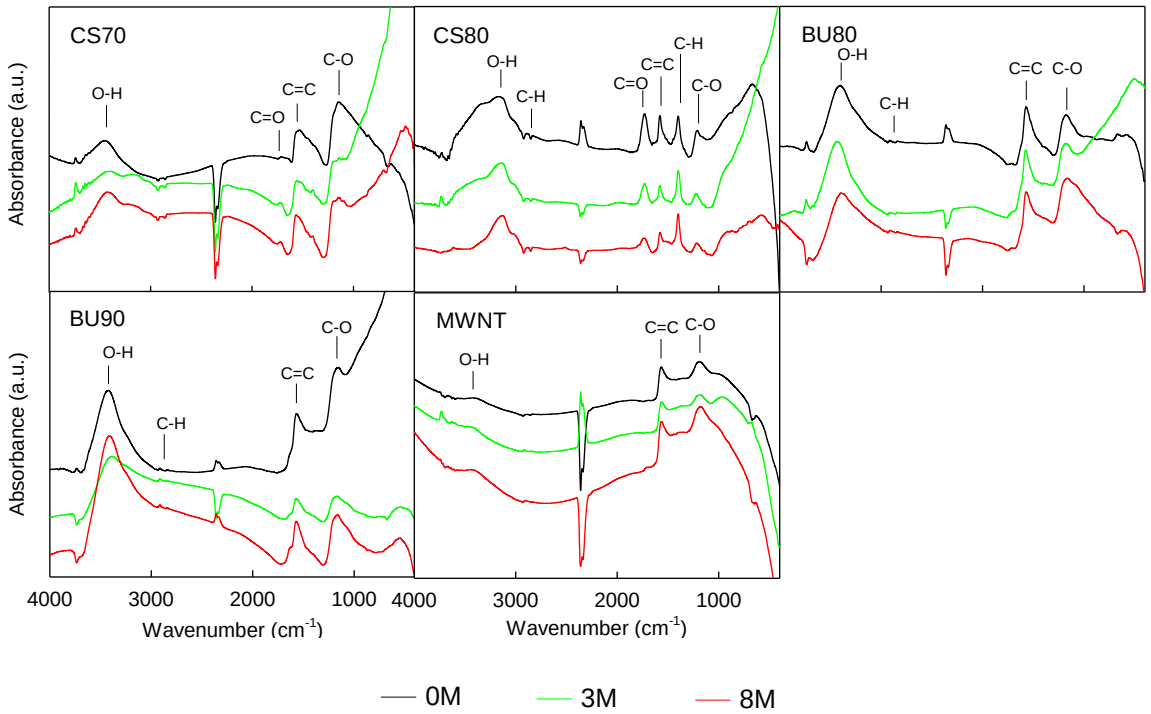

Figure 3.17 Surface chemistry of nanocarbons in aging with 37 ^{o}C for 8 months

At this point, it is important to see that the changes of chemical properties including oxygen, functional groups and defects in 37°C were very similar with what they were in ambient condition (17-24M). The decrease of oxygen/functional groups and defects in CS70, CS80 are most likely due to their metastability and low humidity while other three samples had been fully aged and were not affected any more. It suggests that just increase of temperature from 20°C to 37°C (the actual humidity was quite close to each other in two conditions) could not affect chemical properties of nanocarbons very greatly. The decrease of surface area and pore volume in the beginning months could be explained by the decrease of defects. However, the increase of surface area and pore volume in 3-13 months may be related to other reasons. One possible reason is the higher temperature softened intertubular interaction (van-der-Waals) in carbon nanotubes [81-83]. Thomsen et al. used Raman spectroscopy to analyze temperature

dependent of intertubular interaction (171 cm^{-1}) in SWNT and they found that the diameter between tubes could be enlarged with increasing temperature from 20K to 300K **(Fig. 3.18)** [82]. SWNTs are existed as bundles in which contain lots of carbon tubes. The interstitial channel (site between tubes) could offer an large part of surface area **(Fig. 1.7)** [26, 27], therefore, the increase in intertubular diameter could create more space for N_2 adsorption which lead to increase of surface area and pore volume. Raravikar et al. also conducted similar research with temperature from 299K to 773K, and they concluded that the intertubular interaction is dominated in the process of thermal expansion [83]. Li et al. observed that this kind of thermal expansion effect is more obvious in SWNT than MWNTs. This observation is perfectly matching the results in present research. It was clearly that surface area and pore volume in four SWNTs were changed much greater than they were in MWNTs. The effect of temperature on the physical properties on nanocarbons deserves more research work.

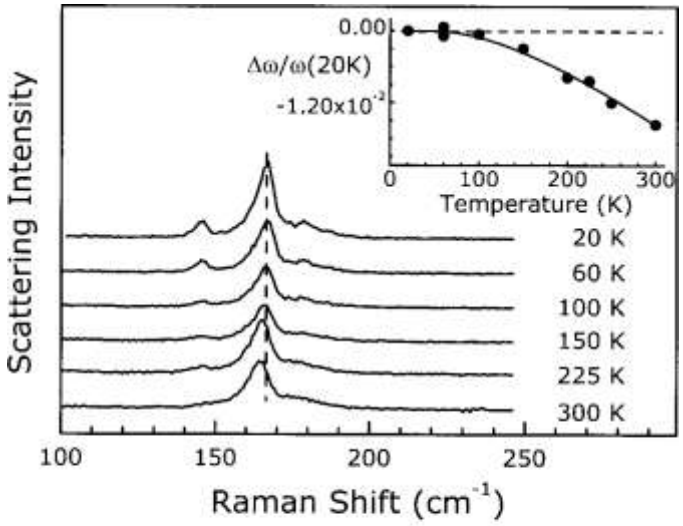

3.18 Raman shift at different temperature

Note: Raman shift = 12.5 +223.5/Diameter

3.2.3 Summary

In this study, five nanocarbons which had been fully aged in ambient condition were moved to an oven with 37°C temperature, and the actual humidity inside of oven was known to be a little bit lower than outside lab condition. Physicochemical properties of nanocarbons were tracked by N_2 adsorption technology, XPS, Raman, and FT-IR. The study showed that chemical properties in this condition were quite similar with those in the ambient conditions (17-24M). The oxygen contents, functional groups and defects were slightly reduced in CS70/CS80, while other three samples were almost unchanged. These decreases were caused probably due to nanocarbons were metastable materials and were still not stable after 16 month of aging in ambient conditions. The decrease of oxygen/functional groups may also be enhanced by the low humidity. The physical properties of nanocarbons, however, were quite different. Surface area and pore volume were decreased in the beginning 1-3 months but were strongly increased in 3-13 months. We deduce the decrease in the beginning months could be resulted by the decrease of defects, however, the increase in 3-13 months may be related with other reasons. The softening of intertubular interaction which could lead to enlargement of interstitial channels between tubes could be a reasonable explanation.

CHAPTER 4

Conclusions

In the present study, we researched effect of ambient temperature and humidity on aging of nanocarbons. Three aging conditions, including ambient condition, 90%RH and 37°C temperature, were set to age nanocarbons. Several commercially available carbon nanotubes and fullerenes (C60) purchased from different companies were researched. Nanocarbons were first aged in the ambient lab condition, which was ~20°C and 40-60%RH; the aging process was conducted from Sep.2006 to Sep.2008. In March 2008 (samples were already aged for 16 months), a small part (60-100mg) of aged samples were moved to two other different aging environments, one with 90%RH and another with 37°C temperature. In 90%RH condition, the temperature was just ambient lab temperature; and in 37°C condition, actual humidity in the oven was a little bit lower than lab condition. In each aging condition, samples were analyzed by N_2 adsorption technology, XPS, Raman, (and FT-IR) periodically. The physicochemical properties, including surface area, pore volume, oxygen content, functional groups, and structural defects, were analyzed. The effects of humidity and temperature on physicochemical properties of nanocarbons were discussed. Several interesting results were obtained from this research and were summarized as follows:

1. In ambient condition, we found that SWNTs exhibit a trend of decreasing surface area and pore volume up to 7 to 15 months but then stabilized, no longer being impacted by

sample age or outgassing temperatures. We also observed a trend of decreasing surface oxygen in all samples from the beginning with much lower % oxygen observed between 12 to 15 months of aging under ambient conditions. The surface oxygen then stabilized for the duration of the study. There was also evidence that the total structural-defect concentration was somehow lowered during the aging process. The decrease in surface oxygen is an unexpected phenomenon because most other carbons, such as activated carbons or carbon molecular sieves, either oxidize or remain unaffected by age. We conclude that nanocarbons are meta-stable materials, and that their aging in ambient conditions has an unexpected effect whereby oxygen leaves their surface, the structure repairs itself and they become more thermodynamically stable with fixed properties.

2. In 90%RH environment, we found that surface area/pore volume and defects of all five nanocarbons were reduced with a trend of approaching to equilibrium. We also observed that the fully aged nanocarbons (in ambient condition) were further functionalized. The high relative humidity promoted chemisorption of oxygen and/or water in the air to nanocarbons which lead to the increase of % oxygen. The changing concentration of functional groups was also supported by FT-IR analysis. This study showed that self-repair of nanocarbons and chemisorption of oxygen and/or water to nanocarbons would be in working together in the 8-month aging process. Given the decrease of defects, we conclude that previous unoccupied defect sites should be the locations where carbon atoms were oxidized in this condition.

3. In 37°C condition, we found that chemical properties of five nanocarbons were quite similar with those in ambient conditions (17-24M). The oxygen contents, functional groups and defects were slightly reduced in CS70/CS80, while other three samples were almost unchanged. These decreases were caused probably due to nanocarbons were metastable materials and were still not totally stable after 16 month of aging in ambient conditions. The decrease of oxygen/functional groups may be caused by lower humidity. The physical properties of nanocarbons, however, were quite different. Surface area and pore volume were decreased in the beginning 1-3 months but were strongly increased in 3-13 months. We deduce the decrease in the beginning months could be resulted by the decrease of defects, however, the increase in 3-13 months may be related with other reasons. The softening of intertubular interaction which could lead to enlargement of interstitial channels between tubes could be a reasonable explanation.

In all, this work studied aging of nanocarbons in three conditions and showed that ambient humidity and temperature could affect the physicochemical of nanocarbons greatly. Also, the nanometric scale of nanocarbons could not only accelerate aging but also make nanocarbons different from bulk carbon materials. The importance of this study is that we find physicochemical properties of nanocarbons were affected by aging timing and also by aging conditions. Thus, this study could benefit potential applications of nanocarbons and help understanding their environmental impacts in the long term.

APPENDICES

APPENDIX - I

Assignments of peaks with functional group in XPS C1s deconvolution

Publications	Author	CNs	Ni-C	sp2	sp3	C-O	C=O	COO	p-p
PHYS. REVIEW **1996**	Javier			284.3	285.2				
J. Phys. Chem. B **1999**	H.Ago	MWNT		284.5	285.2	286.2	287.5	288.9	
Applied Surface **2001**	Lee	SWNT		285		286.4	287.7	288.9	
Carbon **2002**	Boehm	SWNT		284.38					
Fluorine Che. **2003**	Young	SWNT		284.3	285.0			288.5	
Carbon **2003**	M.T	SWNT		284.6		286.3	287.6	288.8	291
Chem. Mater. **2004**	Fang	SWNT		284.3	285.2	286.1	287.6	288.9	
Nanotechnology **2004**	Vast	MWNT		284.6	285.3	286.1	287.4	289.0	291
Carbon **2005**	Okpalugo	MWNT		284.38 –284.5	285.1–285.5	286.2–287.5	286.45 –287.9	288.4–289.54	
Manu		-	283.9						

APPENDIX - II

Assignments of peaks with functional group in FT-IR

Ref	Mate.	O-H	C-H	CH2	C=C	O=C-OH			O=C-H		C-OH	
						C=O	C-O	O-H	C=O	C-H	C-O	O-H
1			3300		1595				1720			
2	CNT	3500			1580	1730						
3	SWNT								1720			
4	SWNT	3463				1710				2695-2830		
5	MWNT					1717		3431				
6	MWNT	3400			1635	1740	1300		1710			
7	MWNT	3500							1710			
8	MWNT	3420	2920	2854					1680			
9	Carbon		2600-3000			1665-1760	1120-1200	2500-3300	I740-I880		1049-1276	3200-3640
10	Carbon					1705-1720	1210-1320	2500-3300	1710-1740	2690-2840	970-1250	3200-3550

APPENDIX - III

TEM of nanocarbons

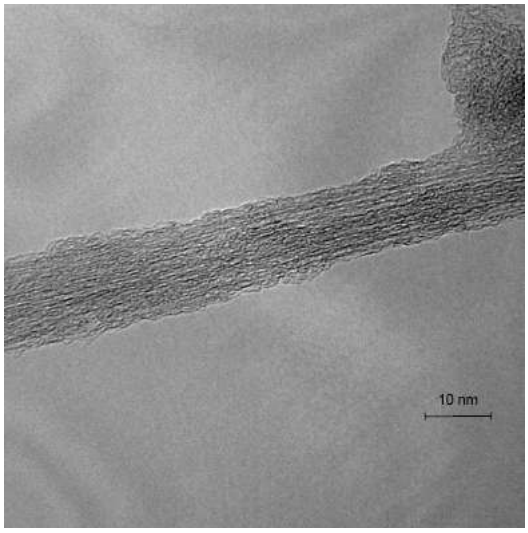

CS70

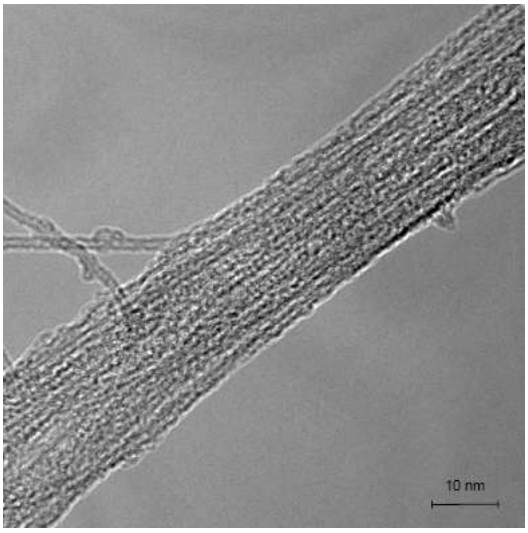

BU90

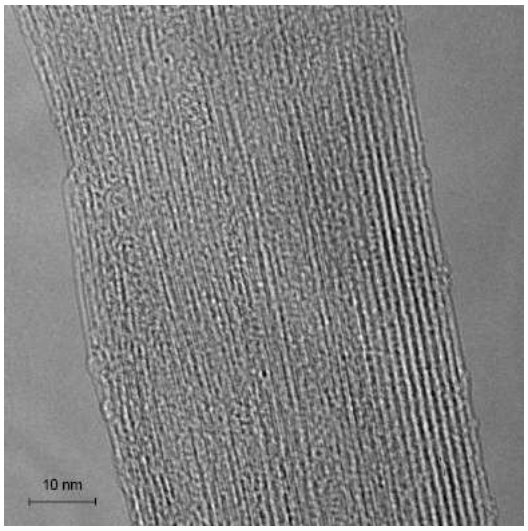

EA95

LIST OF REFERENCES

1. Lijima, S., *Helical microtubules of graphitic carbon.* Nature, 1991. **354**(6348): p. 3.

2. Lijima, S. and T. Lchihashi, *Single-shell carbon nanotubes of 1-nm diameter.* Nature, 1993. **363**: p. 3.

3. Dresselhaus, M.S., G. Dresselhaus, and R. Saito, *Physics of carbon nanotubes.* Carbon, 1995. **33**(7).

4. Ajie, H., et al., *Characterization of the Soluble All-Carbon Molecules C60 and C70.* Journal of Physical Chemistry, 1990. **94**(24): p. 4.

5. Kroto, H.W., et al., *C60: Buckminsterfullerene.* Nature, 1985. **318**(14): p. 2.

6. Dresselhaus, M.S. and P.C. Eklund, *Phonons in carbon nanotubes.* Advances in Physics, 2000. **49**(6): p. 10.

7. Cinke, M., et al., *Pore structure of raw and purified hiPco single-walled carbon nanotubes.* Chemical Physics Letters, 2002. **365**: p. 6.

8. Ebbesen, T.W., et al., *Electrical conductivity of individual carbon nanotubes.* Nature, 1996. **382**: p. 3.

9. Thess, A., et al., *Crystalline ropes of metallic carbon nanotubes* Science, 1996. **273**: p. 5.

10. Charlier, J.-C., *Defects in carbon nanotubes.* Accounts of Chemical Research, 2002. **35**: p. 7.

11. Treacy, M.M.J., T.W. Ebbesen, and J.M. Gibson, *Exceptionally high Young's modulus observed for individual carbon nanotubes.* Nature, 1996. **381**(6584): p. 3.

12. Kong, J., et al., *Nanotube molecular wires as chemical sensors.* Science, 2000. **287**(5453): p. 4.

13. Sankaran, M. and B. Viswanathan, *Hydrogen storage in boron substituted carbon nanotubes.* Carbon, 2007. **45**: p. 8.

14. Yildirim, T. and S. Ciraci, *Titanium-decorated carbon nanotubes as a potential high-capacity hydrogen storage medium.* Physical Review letters, 2005. **94**(17).

15. Sone, H., et al., *Affinity-based elimination of aromatic VOCs by highly crystalline multi-walled carbon nanotubes.* Talanta, 2008. **74**(6): p. 1265.

16. Salipira, K.L., et al., *Carbon nanotubes and cyclodextrin polymers for removing organic pollutants from water.* Environmental Chemical letters, 2007. **5**: p. 5.

17. Peigney, A., et al., *Specific surface area of carbon nanotubes and bundles of carbon nanotubes.* Carbon, 2000. **39**: p. 8.

18. Vast, L., et al., *Chemical functionalization by a fluorinated trichlorosilane of multi-walled carbon nanotubes.* Nanotechnology, 2004. **15**: p. 5.

19. Lafi, L., D. Cossement, and R. Chahine, *Raman spectroscopy and nitrogen vapour adsorption for the study of structural changes during purification of single-wall carbon nanotubes.* Carbon, 2005. **43**: p. 9.

20. Behler, K., et al., *Effect of thermal treatment on the structure of multi-walled carbon nanotubes.* Journal of Nanoparticle Research, 2006. **8**: p. 11.

21. Zhang, J., et al., *Effect of chemical oxidation on the structure of single-walled carbon nanotubes.* Journal of Physical Chemistry B, 2003. **107**: p. 7.

22. Simmons, J.M., et al., *Effect of ozone oxidation on single-walled carbon nanotubes.* Journal of physical Chemistry B, 2006. **110**: p. 6.

23. Yeung, C.S., L.V. Liu, and Y.A. Wang, *Adsorption of small gas molecules onto Pt-doped single-walled carbon nanotubes.* Journal of Physical Chemistry C, 2008. **112**: p. 11.

24. Fedorov, A.S., P.B. Sorokin, and A.A. Kuzubov, *Ab initio study of hydrogen chemical adsorption on platinum surface/carbon nanotube join system.* Physica Status Solidi B-Basic Solid State Physics, 2008. **245**: p. 6.

25. Agnihotri, S., et al., *Theoretical and experimental investigation of morphology and temperature effects on adsorption of organic vapors in single-walled carbon nanotubes.* Journal of Physical Chemistry B, 2006. **110**: p. 8.

26. Agnihotri, S., et al., *Adsorption site analysis of impurity embedded single-walled carbon nanotube bundles.* Carbon, 2006. **44**: p. 8.

27. Agnihotri, S., et al., *Practical modeling of heterogeneous bundles of single-walled carbon nanotubes for adsorption applications: estimating the fraction of open-ended nanotubes in samples.* Journal of Physical Chemistry C, 2007. **111**: p. 9.

28. Buzea, C., I.I. Pacheco, and K. Robbie, *Nanomaterials and nanoparticles: sources and toxicity.* Biointerphases 2007. **2**: p. 55.

29. Nel, A., et al., *Toxic potential of materials at the nanolevel.* Science, 2006. **311**: p. 6.

30. Monteiro-Riviere, N.A., et al., *Multi-walled carbon nanotube interactions with human epidermal keratinocytes.* Toxicology Letters 2005. **155**: p. 8.

31. Muller, J., et al., *Respiratory toxicity of multi-wall carbon nanotubes.* Toxicology and Applied Pharmacology, 2005. **207**: p. 11.

32. Oberdörster, G., et al., *Translocation of inhaled ultrafine particles to the brain.* Inhalation Toxicology, 2004. **16**: p. 9.

33. Jia, G., et al., *Cytotoxicity of carbon nanomaterials: single-wall nanotube, multi-wall nanotube, and fullerene.* Envronmental Science & Technology, 2005. **39**: p. 6.

34. Tian, F., et al., *Cytotoxicity of single-wall carbon nanotubes on human fibroblasts.* Toxicology in Vitro, 2006. **20**: p. 11.

35. Shvedova, A.A., et al., *Exposure to carbon nanotube material: assessment of nanotube cytotoxicity using human keratinocyte cells.* Journal of Toxicology and Environmental Health, Part A, 2003. **66**: p. 18.

36. Lam, C.-W., et al., *Pulmonary toxicity of single-wall carbon nanotubes in mice 7 and 90 days after intratracheal instillation.* Toxicological Sciences, 2004. **77**: p. 9.

37. Sayes, C.M., et al., *The differential cytotoxicity of water-soluble fullerenes.* Nano Letters, 2004. **4**: p. 7.

38. Sayes, C.M., et al., *Functionalization density dependence of single-walled carbon nanotubes cytotoxicity in vitro.* Toxicology Letters, 2006. **161**: p. 8.

39. Kang, S., M.S. Mauter, and M. Elimelech, *Physicochemical determinants of multiwalled carbon nanotube bacterial cytotoxicity.* Environmental Science & Technology, 2008. **42**: p. 7.

40. Healy, M.L., L.J. Dahlben, and J.A. Isaacs, *Environmental assessment of single-walled carbon nanotube processes.* Journal of Industrial Ecology, 2008. **12**: p. 18.

41. Wiesner, M.R., et al., *Assessing the risks of manufactured nanomaterials.* Environmental Science & Technology, 2006. **40**: p. 10.

42. Deng, X., et al., *Translocation and fate of multi-walled carbon nanotubes in vivo.* Carbon, 2007. **45**: p. 6.

43. Fernando, K.A.S., Y. Lin, and Y.-P. Sun, *High aqueous solubility of functionalized single-walled carbon nanotubes.* Langmuir, 2004. **20**: p. 2.

44. Saleh, N.B., L.D. Pfefferle, and M. Elimelech, *Aggregation kinetics of multiwalled carbon nanotubes in aquatic systems: measurements and environmental implications.* Environmental Science & Technology, 2008. **42**: p. 7.

45. Puri, B.R., *Proceeding of the 5th Conference on Carbon, Vol.I.* 1962, New York: Pergamon Press.

46. Lagorsse, S., F.D. Magalhães, and A. Mendes, *Aging study of carbon molecular sieve membranes.* Journal of Membrane Science, 2008. **310**: p. 9.

47. Menendez, I. and A.B. Fuertes, *Aging of carbon membranes under different environments.* Carbon, 2001. **39**: p. 8.

48. Petit, J.C. and Y. Bahaddi, *New insight on the chemical role of water vapor in the ageing of activated carbon.* Carbon, 1993. **31**: p. 5.

49. Agnihotri, S., M. Rostam-Abadi, and M.J. Rood, *Temporal changes in nitrogen adsorption properties of single-walled carbon nanotubes.* Carbon, 2004. **42**: p. 12.

50. Sayago, I., et al., *Novel selective sensors based on carbon nanotube films for hydrogen detection.* Sensors and Actuators B, 2007. **122**: p. 6.

51. Lam, C.-w., et al., *A review of carbon nanotube toxicity and assessment of potential occupational and environmental health risks.* Critical Reviews in Toxicology, 2006. **36**: p. 29.

52. Warheit, D.B., et al., *Comparative pulmonary toxicity assessment of single-wall carbon nanotubes in rats.* Toxicology Science, 2004. **77**: p. 9.

53. A.Shvedova, A., et al., *Unusual inflammatory and fibrogenic pulmonary responses to single-walled carbon nanotubes in mice.* American Journal of Physiology. Lung Cell Molecular Physiology, 2005. **289**: p. 11.

54. Brunauer, S., P.H. Emmett, and E. Teller, *Adsorption of gases in multimolecular layers.* Journal of the American Chemical Society, 1938. **60**(2): p. 12.

55. *Autosorb-1 Operating Manual*. 2005, Boynton Beach: Quantachrome Instruments.

56. Hollander, J.M. and W.L. Jolly, *X-Ray photoelectron spectroscopy.* Accounts of chemical research 1970. **3**.

57. Vast, L., et al., *Chemical functionalization by a fluorinated trichlorosilane of multi-walled carbon nanotubes.* Nanotechnology 2004. **15**: p. 5.

58. Fang, H.-T., et al., *Purification of single-wall carbon nanotubes by electrochemical oxidation.* Chemistry of Materials, 2004. **16**: p. 7.

59. Ago, H., et al., *Work functions and surface functional groups of multiwall carbon nanotubes.* Journal of Physical Chemistry B, 1999. **103**: p. 6.

60. Ramma, M., et al., *Studies of amorphous carbon using X-ray photoelectron spectroscopy, near-edge X-ray-absorption fine structure and Raman spectroscopy.* Thin Solid Films, 1999. **354**: p. 5.

61. Kim, U.J., et al., *Raman and IR spectroscopy of chemically processed single-Walled Carbon Nanotubes.* 2005.

62. Wikipedia. *http://en.wikipedia.org/wiki/Raman_spectroscopy*.

63. Antunes, E.F., et al., *Comparative study of first- and second-order Raman spectra of MWCNT at visible and infrared laser excitation.* Carbon, 2006. **44**: p. 10.

64. Rao, A.M., et al., *Diameter-selective Raman scattering from vibrational modes in carbon nanotubes.* Science, 1997. **275**: p. 5.

65. Dillon, A.C., et al., *Systematic inclusion of defects in pure carbon single-wall nanotubes and their effect on the Raman D-band.* Chemical Physics Letters 2005. **401**: p. 7.

66. Bag, D.S., et al., *Chemical functionalization of carbon nanotubes with 3-methacryloxypropyltrimethoxysilane (3-MPTS).* Smart Materials and Structures, 2004. **13**: p. 5.

67. Kim, U.J., et al., *Raman and IR Spectroscopy of Chemically Processed Single-Walled Carbon Nanotubes.* Journal of American Chemical Society, 2005. **127**: p. 9.

68. Kumar, N.A., et al., *Preparation of poly 2-hydroxyethyl methacrylate functionalized carbon nanotubes as novel biomaterial nanocomposites.* European Polymer Journal, 2008. **44**: p. 8.

69. Xie, X. and L. Gao, *Characterization of a manganese dioxide/carbon nanotube composite fabricated using an in situ coating method.* Carbon, 2007. **45**: p. 9.

70. Chen, C.-H. and C.-C. Huang, *Enhancement of hydrogen spillover onto carbon nanotubes with defect feature.* Microporous and Mesoporous Materials, 2008. **109**: p. 11.

71. Robinson, J.A., et al., *Role of defects in single-walled carbon nanotube chemical sensors.* Nano Letters, 2006. **6**: p. 5.

72. Horner, D.A., et al., *Increased reactivity of single wall carbon nanotubes at carbon ad-dimer defect sites.* Chemical Physics Letters, 2007. **450**: p. 5.

73. Wang, C., et al., *Chemical functionalization of carbon nanotubes by carboxyl groups on stone-wales defects: a density functional theory study.* Journal of Physical Chemistry B, 2006. **110**: p. 6.

74. Billinge, B., J. Docherty, and M. Bevan, *The desorption of chemisorbed oxygen from activated carbons and its relationship to aging and methyl-iodide retention efficiency.* Carbon, 1984. **22**(1).

75. Billinge, B. and M. Evans, *The growth of surface oxygen complexes on the surface of activated carbon exposed to moist air and their effect on methyl iodide-131 retention.* Journal de chimie physique, 1984. **81**.

76. Adams, L.B., et al., *An examination of how exposure to humid air can result in changes in the adsorption properties of activated carbon.* Carbon, 1987. **26**(4): p. 9.

77. Itay, M., C.R. Hill, and D. Glasser, *A Study of The Low Temperature Oxidation of Coal.* Fuel Processing Technology, 1989. **21**: p. 17.

78. Pierce, C., et al., *Adsorption of water by carbon.* Journal of the American Chemical Society 1951. **73**.

79. Smith, R.N., C. Pierce, and C.D. Joel, *The low temperature reaction of water with carbon.* The Journal of Physical Chemistry, 1954. **58**: p. 5.

80. Garcia-Perez, J.V., et al., *Water sorption isotherms for lemon peel at different temperatures and isosteric heats.* LWT, 2008. **41**: p. 8.

81. Li, H.D., et al., *Temperature dependence of the Raman spectra of single-wall carbon nanotubes.* APPLIED PHYSICS LETTERS, 2000. **76**(15): p. 2053.

82. Thomsen, C., et al., *Intermolecular Interaction in Carbon Nanotube Ropes.* Physica Status Solidi B-Basic Solid State Physics, 1999. **215**(1): p. 7.

83. Raravikar, N.R., et al., *Temperature dependence of radial breathing mode Raman frequency of single-walled carbon nanotubes.* PHYSICAL REVIEW B, 2002. **66**.

VITA

Liangcheng Yang was born on June 15, 1983 in wenzhou, China. He completed high school education at Pingyang No.1 School and enrolled at Zhejiang University for his undergraduate studies in Environment Science in 2001. At Zhejiang Univ., he participated in several summer intern programs as research assistant. Upon receiving his BS degree in 2005, Liangcheng took a process engineer position in SanHe Environmental Engineering & Technology Ltd. in Hangzhou for two years before returning to school for graduate studies in Environment Engineering at The University of Tennessee, Knoxville. He graduated August 2009 with an M.S degree and has accepted a PhD program offer from Agricultural and Biological Engineering department in University of Illinois at Champaign Urbana.